arXiv:0908.4133v2 [astro-ph.CO] 11 Dec 2009

Mon. Not. R. Astron. Soc. **000**, 1–31 (2009) Printed 11 December 2009 (MN LaTeX style file v2.2)

Tracers of stellar mass-loss. I. Optical and near-IR colours and surface brightness fluctuations

Rosa A. González-Lópezlira[1] ∗, Gustavo Bruzual A.[2], Stéphane Charlot[3,4] Javier Ballesteros-Paredes[1] and Laurent Loinard[1]

[1] *Centro de Radioastronomía y Astrofísica, Universidad Nacional Autónoma de México,*
Apdo. Postal 72-3 (Xangari), Morelia, Michocán 58089, México
[2] *Centro de Investigaciones de Astronomía, Apartado Postal 264, Mérida 5101-A, Venezuela*
[3] *UPMC Univ Paris 06, UMR7095, Institut d'Astrophysique de Paris, F-75014, Paris, France*
[4] *CNRS, UMR7095, Institut d'Astrophysique de Paris, F-75014, Paris, France*

Submitted to MNRAS, 11 December 2009

ABSTRACT

We present optical and IR integrated colours and SBF magnitudes, computed from stellar population synthesis models that include emission from the dusty envelopes surrounding TP-AGB stars undergoing mass-loss. We explore the effects of varying the mass-loss rate by one order of magnitude around the fiducial value, modifying accordingly both the stellar parameters and the output spectra of the TP-AGB stars plus their dusty envelopes. The models are single burst, and range in age from a few Myr to 14 Gyr, and in metallicity between $Z = 0.0001$ and $Z = 0.07$; they combine new calculations for the evolution of stars in the TP-AGB phase, with star plus envelope SEDs produced with the radiative transfer code DUSTY. We compare these models to optical and near-IR data of single AGB stars and Magellanic star clusters. This comparison validates the current understanding of the role of mass-loss in determining stellar parameters and spectra in the TP-AGB. However, neither broad-band colours nor SBF measurements in the optical or the near-IR can discern global changes in the mass-loss rate of a stellar population. We predict that mid-IR SBF measurements can pick out such changes, and actually resolve whether a relation between metallicity and mass-loss exists.

Key words: stars: AGB and post–AGB — stars: carbon — stars: mass-loss — Magellanic Clouds — infrared: stars — stars: circumstellar matter — stars: evolution — galaxies: evolution — galaxies: stellar content

Online-only material: machine-readable and VO tables

1 INTRODUCTION.

Stellar mass-loss is inseparable from stellar evolution and death. It is fundamental to inject enriched material into the interstellar medium, and hence a major driver of the chemical enrichment and evolution of galaxies. Whereas the energetic photons emitted by massive, young stars destroy molecular gas, the dense outflows of evolved stars return to the ISM both molecular gas and dust grains where more H_2 can then form. Mass-loss is especially important at the tip of the asymptotic giant branch (AGB) for intermediate-mass stars ($1M_\odot \lesssim M_{ZAMS} \lesssim 9M_\odot$). Consequently, mass-loss plays a central role also in shaping the AGB and planetary nebula luminosity functions. It determines the white dwarf mass spectrum and cooling times, and the minimum supernova (SN) progenitor mass. Mass-loss thus influences the rate of SNe types II, Ib, and Ic, and possibly determines the mass of SNe Type Ia progenitors and impacts their frequency (Bowen & Willson 1991; Willson 2000).

Thermally-pulsing AGB (TP-AGB) stars are the most luminous red stars in intermediate-age stellar populations, and accordingly affect their integrated properties. The relevance of AGB stars contrasts with our inadequate understanding of this evolutionary phase. The TP-AGB has proven especially hard to model, on account of the thermal

---

∗ e-mail: `r.gonzalez@crya.unam.mx`

pulses they suffer; the convective dredge-up of processed heavy elements to the stellar surface; and the ejection of the stellar envelope that ends the phase (Bruzual & Charlot 2003). There is an extensive bibliography dealing with the difficulties in treating the TP-AGB (e.g., Renzini & Voli 1981; Iben & Renzini 1983; Marigo et al. 1996; Maraston 1998, 2005). In particular, the relation between the fundamental parameters (luminosity, L; mass, M; and metallicity, Z) of the central star and the mass-loss rate, $\dot{M}$, is not quite well understood and, therefore, controversial. Of course, it does not help that the dust in the ejected envelopes precludes the direct observation of the stellar photospheres. Data with relatively good spatial resolution of the dusty cocoons themselves, on the other hand, have been available only in the last decade, with the arrival of the Infrared Space Observatory (ISO) and, presently, the Spitzer Space Telescope.

Customarily, $\dot{M}$ has been described by the empirical Reimers' law (Reimers 1975, 1977), written as $\dot{M} = \eta LR/M$; $R(L, M, Z)$ is the stellar radius, and η is a fitting parameter. Modifications to this law, motivated by the large scatter of observationally determined mass-loss around the Reimers' relation, have been proposed by, among others, Baud & Habing (1983), Bloecker (1995), and Groenewegen & de Jong (1994). Those working on the detailed modeling of mass-loss at the TP-AGB have countered that, in actuality, stellar luminosity first increases at constant mass until the star reaches a "cliff" in the log M vs. log L plane; after this point, mass-loss depends much more steeply on stellar parameters than stated by empirical relations, such that the stellar envelope is lost nearly exponentially in time at roughly constant luminosity (Bowen 1995; Willson 2000, her Fig. 7, and references therein). In this view, empirical relations are the result of very strong selection effects, and only reflect the fact that mass-loss rates are measurable for just a fraction of the stars undergoing mass-loss at any given time. Thus, in the log $\dot{M}$ vs. LR/M plane, the so-called cliff and Reimers' relation are almost coincident (see Fig. 8 of Willson 2000). Before reaching the cliff, stars have low, unmeasurable mass-loss rates; conversely, the stage beyond the cliff is short-lived, and most likely stars will be highly obscured behind a dusty envelope. A sample of stars with observable mass-loss rates should include, according to Willson (2000), mainly objects within one dex in $\dot{M}$ of the cliff.

The purpose of this paper is to produce population synthesis models that include different mass-loss rates in the TP-AGB. To this end, we combine stellar population evolutionary models with theoretical spectral energy distributions (SEDs) that take into account the radiative transfer in the dusty circumstellar envelopes. To begin with, the SEDs are calculated on the basis of the mass-loss rates included in the evolutionary tracks; we then produce SEDs for the same stellar types, but with mass-loss rates one order of magnitude above and below the rates in the tracks, in order to explore the whole range where mass-loss is observable in the optical. Finally, we confront the resulting theoretical broadband colours and fluctuation magnitudes with optical and near-IR observations of AGB stars and Magellanic star clusters.

2 STELLAR POPULATION SYNTHESIS MODELS AND $\dot{M}$.

In this paper we use a preliminary version of the Charlot & Bruzual (2009; CB09 henceforth) simple stellar population (SSP) evolutionary synthesis models to compute isochrones in the age range from a few Myr to 14 Gyr, and metal (helium) content $Z(Y)$ = 0.0001(0.26), 0.0004(0.26), 0.001(0.26), 0.002(0.26), 0.004(0.26), 0.008(0.26), 0.017(0.26), 0.04(0.30), and 0.07(0.34). The CB09 models are formally identical to the Bruzual & Charlot (2003; BC03 hereafter) models, but include several important improvements. Firstly, up to $15 M_{\odot}$ and for the metal and He contents indicated above, CB09 use the tracks from the models with updated input physics by Bertelli et al. (2008). For stars more massive than $15 M_{\odot}$, in the range from 20 to $120 M_{\odot}$, CB09 use the so-called Padova 1994 tracks (Alongi et al. 1993; Bressan et al. 1993; Fagotto et al. 1994a,b; Girardi et al. 1996).

Secondly, in the CB09 models used in this paper, the TP-AGB evolution of low- and intermediate-mass stars is followed according to the prescription of Marigo & Girardi (2007). This semi-empirical prescription includes several important theoretical improvements over previous calculations, and it has been calibrated using carbon star luminosity functions in the Magellanic Clouds (MC) and TP-AGB lifetimes (star counts) in MC clusters (we refer to the paper by Marigo & Girardi for details). The reader should be aware that Bertelli et al. (2008) use a different set of TP-AGB tracks, also based on the Marigo & Girardi (2007) prescription, but extrapolated to different chemical compositions of the stellar envelope. These sets of TP-AGB tracks are un-calibrated, as pointed out by Bertelli et al. (2008), since no attempt was made to reproduce the available observations. CB09 will discuss the differences introduced in the evolutionary models by the use of the calibrated or the un-calibrated TP-AGB tracks from these authors.

Thus, the CB09 models discussed here use the tracks in the Bertelli et al. (2008) atlas up to the end of the AGB phase, and extend these tracks with the results of Marigo & Girardi (2007) to cover the TP-AGB phase. Bruzual (2007) has shown that models computed following the Marigo & Girardi (2007) prescription have brighter K-band magnitudes and redder near-IR colours than other models, e.g., BC03, that use a semi-empirical treatment of the TP-AGB evolution based on an older empirical calibration of the lifetime of these stars, and an educated guess of the mass associated to TP-AGB stars of a given luminosity.[1]

The Marigo & Girardi prescription, as implemented by CB09, accounts for 15 evolutionary stages in the TP-AGB (six in the O-rich phase, six in the C-rich phase, and three in the superwind phase). By contrast, the BC03 models include only one evolutionary stage at each of these phases. The signature of TP-AGB stars, i.e., the red colour of the integrated SSP around 1 Gyr, becomes more relevant in the CB09 models than in previous computations by BC03 and other authors (e.g., Maraston et al. 2006). For $Z = 0.008$, the TP-AGB stars in the CB09 models contribute close to a factor of two more light in the K-band than in the BC03 models. At maximum, the TP-AGB contributes close to 70% of the K-light in the CB09 model for $Z = 0.008$, but only 40% in the BC03 model. The peak K-band luminosity in the BC03 model occurs at around 1 Gyr, whereas in the CB09 model it stays high and close to constant from 0.1 to 1 Gyr. The evolutionary rate is such that the total number of TP-AGB stars present in the CB09 1 Gyr isochrone is 3.4 times larger than the number of these stars in the BC03 models. The TP-AGB stars represent 0.012% of the total number of stars in this population at this age in the CB09 model, but only 0.0036% in the BC03 model. A 10^6 $M_\odot$ cluster contains 181 TP-AGB stars in the CB09 model, but only 53 of these stars in the BC03 model. The TP-AGB stars are about 0.3 mag brighter at K in the BC03 than in the CB09 isochrone. The net effect of all these factors is an increase of roughly 90% in the contribution of TP-AGB stars to the total K flux of the $Z = 0.008$ SSP at this age. See Bruzual (2007) for more details.

---

[1] We refer to the papers by Marigo & Girardi and BC03 for details. In particular, Girardi & Marigo (2007) derive constraints on TP-AGB lifetimes, while Marigo & Girardi (2007) compare their theoretical initial-final mass relation with empirical data of white dwarfs in open clusters and binary systems.

The CB09 isochrones provide, at any given age, the number of stars at each of 310 positions in the $(L_{BOL}, T_{\rm eff})$ plane. To each star along the isochrone, an SED is assigned from the Westera et al. (2002) stellar library for all stellar phases, except for the C-rich and superwind stages of the TP-AGB; for these we use several options, including the DUSTY models already mentioned above. For each of the nine stellar metallicities considered, we have calculated CB09 models for four possible choices of the SED assigned to TP-AGB stars in the superwind phase: (1) the SEDs used in the BC03 and CB09 models (standard models hereafter),[2] and (2) model spectra computed with the code DUSTY for: (*a*) dusty envelopes that result from the fiducial $\dot{M}$ during these evolutionary phases, (*b*) dusty envelopes from $\dot{M}$ one order of magnitude above fiducial, and (*c*) dusty envelopes from $\dot{M}$ one order of magnitude below fiducial. The input spectra for the DUSTY code are the same spectra used at these phases by CB09, albeit modified according to the updated stellar parameters if the mass-loss-rate is $\dot{M} \times 10$ or $\dot{M}/10$. In all cases we use the Chabrier (2003) IMF.

We then compute the time evolution of several properties of single-burst stellar populations, in particular their integrated fluxes and fluctuation luminosities in the V, B, R, I, J, H, and K_s bands, as well as in the IRAC and MIPS wavelengths observed by the Spitzer Space Telescope (Section 4).[3]

Besides predicting stellar time evolution on the Hertzsprung-Russell diagram, the new Marigo & Girardi models self-consistently estimate pulsation modes and periods, changes in the chemical composition of the stellar envelopes and, most relevant for the present work, mass-loss rates owing to the pulsating, dust driven winds of O- and C-rich AGB stars. In the case of O-rich stars, Marigo & Girardi (2007) derive luminosities from M, R, and pulsation period (P); next, they calculate stellar mass-loss rates according to the stars' evolutionary slopes d (log M)/ d (log L), on the basis of the Bowen & Willson (1991) dynamical atmospheres for Miras including dust.[4] The Bowen & Willson (1991) models anticipate that mass-loss rates of O-rich stars diminish with decreasing metallicity, due to a less efficient dust production and a smaller photospheric radius at a fixed luminosity. To determine mass-loss rates of C-rich stars, luminosities are calculated first from stellar temperature ($T_{\rm eff}$), M, and P. At low luminosities, mass-loss is driven mostly by stellar pulsation, whereas radiation pressure on dust grains plays a secondary role. However, at a critical luminosity that depends on stellar mass, dust-driven superwinds take place. For the superwind phase, Marigo & Girardi calculate $\dot{M}(T_{\rm eff}, L, M, P, C/O)$ based on the pulsating wind models by Wachter et al. (2002), although including in addition an explicit dependence on the C/O ratio. The mass-loss at each evolutionary stage is then taken into account to consistently determine the stellar parameters in subsequent phases.

Examples of predicted mass-loss rates are presented by Marigo & Girardi (2007) in their Figures 15 and 16. They also note that, for all cases and C/O values: (*a*) $\dot{M}$ is ultimately controlled by the changes in L and $T_{\rm eff}$ linked to He-shell flashes, (*b*) most of the stellar mass-loss occurs during the high-luminosity but quiescent stages that preceed thermal pulses, and (*c*) the superwind regime is achieved during fundamental mode pulsation.

To date, there are few cases where evolutionary synthesis models include the effects of mass-loss in stellar spectra. Among these, Lançon & Mouhcine (2002), Mouhcine & Lançon (2003), and Maraston (2005) use averaged observed SEDs, whereas Bressan et al. (1998) and Piovan et al. (2003) have pioneered the use of analytical relations for the mass-loss rates and wind terminal velocities that then allow them to model the spectra of dusty circumstellar envelopes. We have proceeded in a manner similar to these latter works. For each stellar type in the TP-AGB, SEDs of star plus envelope were produced with the radiative transfer code DUSTY; as was mentioned before, SEDs were also processed for the same stellar types, but with mass-loss rates one order of magnitude above and below the rates in the tracks, in order to explore the whole range where mass-loss is observable in the optical, according to Willson (2000). A change in $\dot{M}$, in turn, entails variations in L and hence stellar lifetime, R, envelope and core masses, $T_{\rm eff}$, pulsation period, dust-to-gas ratio, dust composition, and C/O ratio. A major challenge for this work is that we are aiming at extrapolating mass-loss rates at a large range of metallicities, but in fact a good calibration of all the parameters involved in individual TP-AGB stars exists only for Galactic and Magellanic TP-AGB stars. Two possible routes are open: we can either limit our work to these metallicities, or venture to make predictions for lower and higher metallicities, with the clear caveat that most relations have not been tested in these conditions. We choose the second, and strive to keep as close as possible to the procedures used by Marigo & Girardi (2007) to produce the original stellar tracks.

---

[2] The spectra of TP-AGB stars have not been updated in the preliminary version of the standard CB09 model used here with respect to those used in BC03. For C-type TP-AGB stars and stars in the superwind phase at the end of the TP-AGB evolution, BC03 and CB09 use period-averaged spectra based on models by Schultheis et al. (1999) and observations of Galactic stars. For O-rich TP-AGB stars and stars at the tip of the RGB, BC03 and CB09 use the Westera et al. (2002) atlas. The final version of CB09 will include new spectra for TP-AGB stars.

[3] Strictly speaking, the integrated fluxes and fluctuation luminosities of a stellar population at a given time are not the product of the mass-loss rate at that time (or at any time), but rather the effect of the total mass-loss up to that point.

[4] d (log M)/ d (log L) = 1, and $\dot{M} = 5.67 \times 10^{-7} M_\odot$ yr^{-1} along the "cliff" line; this rate marks the onset of the "superwind" phase.

We present our results in the subsequent sections, while the interested reader can follow our calculations in detail in the Appendix. CB09 models (i.e., with fiducial mass-loss) are reported in tables 1 through 4. Optical and near-IR colours as a function of age, for different chemical compositions, are presented in tables 1 and 2, respectively without and with dusty envelopes; fluctuation amplitudes are listed in tables 3 and 4.

3 BROAD-BAND COLOURS.

3.1 Individual AGB stars.

Fig. 1 displays the theoretical colours[5] of individual stars along the 0.2 Gyr (dotted line), 0.5 Gyr (solid line), and 9.5 Gyr (dashed line) isochrones for populations with four metallicities ($Z = 0.004$, black; 0.008, cyan; 0.017, red; and 0.04, magenta), and our four choices of spectra for stars in the TP-AGB.

As a first test of the models, we compare the theoretical near-infrared (near-IR) broad-band colours to the observed two-colour diagram, $[H-K]$ vs. $[J-H]$, of individual AGB stars in the compilation by Piovan et al. (2003); the sample is shown in Fig. 2. Theoretical colours of individual stars with fiducial (thick lines) and high (thin lines) mass-loss rates are also shown in Fig. 2, superimposed on the observed AGB sample. The metallicity and age symbols are the same as in Fig. 1.

An examination of the bottom left panel of Fig. 1 (SEDs with $\dot{M}/10$) illustrates that a population where TP-AGB stars are nearly devoid of dusty envelopes cannot explain the colour range of observed AGB stars. As for the standard CB09 isochrones (top left panel of Fig. 1), not even the young populations with massive AGB stars reach beyond $[J-H] \sim 3$ and $[H-K_s] \sim 2$. By contrast, there are stars in the sample with both $[J-H]$ and $[H-K_s] > 4$. Models with fiducial $\dot{M}$ and dusty envelopes (top right panel) cover these values comfortably, but only at young ages and with solar or supersolar metallicities. Models with $\dot{M} \times 10$ (bottom right panel) and high metallicities fit the reddest stars regardless of age, whereas for lower Z also young ages are required.

Figures 1 and 2 suggest that some of the stars in the sample with $[H-K_s] \geqslant 2$ could be young (~ 0.2 Gyr old), comparatively massive ($M > 4M_\odot$ at the beginning of the TP-AGB phase), stars with subsolar metallicity, going through a superwind phase with a mass-loss rate of $\sim$ a few $\times 10^{-5} - 10^{4} M_\odot\ \mathrm{yr}^{-1}$, or roughly one order of magnitude above the fiducial rate. Stars could continue losing mass at these rates for $\sim 10^7$ years.

For a more recent example, the 2MASS $[H-K_s]$ vs. $[J-K_s]$ integrated colours of individual AGB candidates in the sample published by Srinivasan et al. (2009) are displayed in Figure 3. Different colours are used for O-rich, C-rich, and "extreme" (based on their 2MASS and IRAC colours) AGB objects. The colour range is smaller than that in Figure 2. This can be better appreciated in Figure 4; now in the same scale as Figure 2, the Srinivasan et al. sample is shown as a cloud of gray points, with our models superimposed. Ages and metallicities of the models are indicated as in Figures 1 and 2. The agreement with the data is similar to that achieved for the older sample compiled by Piovan et al. (2003).

3.2 Star clusters.

Fig. 5 presents theoretical two-colour diagrams, $[H-K_s]$ vs. $[J-H]$, for SSPs with different metallicities ($Z = 0.0004$, blue; 0.008, cyan; 0.017, red) and, again, our 4 choices of mass-loss and spectra for stars in the TP-AGB. The model ages go from 100 Myr to 14 Gyr. The first thing that stands out is the range covered by the colour values. As opposed to the colours of individual stars (see Figures 1, 2, and 4), the integrated colours of SSPs are in general confined to the very small range $0.3 < [J-H] < 1.0$, $0.1 \leqslant [H-K_s] < 0.6$, with $[J-H]$ varying slightly more than $[H-K_s]$, no matter what mass-loss rate is used for the models.

Still, it should be useful to compare the theoretical integrated broad-band colours to those of stellar clusters. Our first test set comprises the MC clusters measured by González et al. (2004); González-Lópezlira et al. (2005). These authors assembled 8 artificial "superclusters", by coadding data of 191 star clusters in bins with similar ages and metallicities, according to classes I − VII in the Searle et al. (1980) SWB categorization scheme, plus an ultra-young (pre-SWB class) supercluster.[6] The purpose of such procedure is to reduce the stochastic uncertainty produced by the inadequate sampling, in sparse clusters, of stars evolving through short evolutionary phases, of which the AGB is a prime example. "Superclusters", therefore, should be more appropriate test objects than individual star clusters (see, for example, Santos & Frogel 1997; Bruzual 2002; Cerviño et al. 2002). In fact, if the assumption is made that the numbers of stars in different evolutionary stages have a Poissonian distribution, then the theoretical relative errors of integrated colours scale as $M_{\mathrm{tot}}^{-1/2}$, where M_{tot} is the total mass of the stellar population (Cerviño et al. 2002). In what follows, we will use coloured regions to represent expected $\pm 1\sigma$ stochastic errors. The MC "supercluster" ages, that go from ~ 6 Myr to > 10 Gyr, are not the originally adopted by González et al. (2004). Instead, we use now the updated calibration by Girardi et al. (1995) of the S-parameter developed by Elson & Fall (1985, 1988); this parameter relates the ages of LMC clusters to their UBV colours. To each supercluster we assign the age that corresponds to the "central" S-type of its constituents; the error is set to span the

---

[5] We use K_s or K, depending on the observations the models will be compared with. The difference is very hardly noticeable.

[6] Individual clusters of each SWB class were centred, sky subtracted, multiplicatively scaled to a common photometric zeropoint and dereddened before coaddition. SMC clusters were magnified to place them at the distance modulus of the LMC.

Table 1. Colours for CB09 models with fiducial mass-loss but without dusty envelopes

Age (Gyr)	$B-V$	$V-R$	$V-I$	$V-J$	$V-H$	$V-K_s$	$V-K$
$Z = 0.017$ $Y = 0.26$							
0.005	-0.142	-0.027	-0.043	-0.115	-0.031	-0.010	-0.017
0.006	-0.063	0.062	0.144	0.339	0.622	0.699	0.681
0.007	-0.059	0.070	0.175	0.443	0.793	0.900	0.878
0.008	-0.075	0.062	0.184	0.524	0.950	1.097	1.071
0.009	-0.133	0.020	0.161	0.604	1.146	1.354	1.324
0.010	-0.138	0.029	0.201	0.721	1.311	1.531	1.499
0.020	-0.071	0.096	0.348	0.967	1.606	1.816	1.781
0.030	-0.021	0.127	0.369	0.931	1.528	1.709	1.677
0.040	0.002	0.126	0.335	0.815	1.353	1.510	1.480
0.050	0.035	0.138	0.339	0.790	1.296	1.437	1.409
0.060	0.051	0.143	0.340	0.777	1.264	1.399	1.372
0.070	0.087	0.165	0.369	0.818	1.291	1.425	1.401
0.080	0.097	0.172	0.381	0.834	1.304	1.437	1.414
0.090	0.117	0.186	0.405	0.869	1.338	1.468	1.446
0.100	0.130	0.196	0.421	0.896	1.368	1.498	1.475
0.200	0.141	0.203	0.498	1.402	2.078	2.345	2.314
0.300	0.171	0.214	0.508	1.302	2.004	2.301	2.304
0.400	0.224	0.234	0.543	1.306	1.986	2.269	2.273
0.500	0.275	0.255	0.587	1.368	2.017	2.262	2.248
0.600	0.311	0.274	0.621	1.412	2.067	2.315	2.302
0.700	0.387	0.309	0.683	1.477	2.142	2.392	2.385
0.800	0.431	0.331	0.716	1.500	2.166	2.415	2.412
0.900	0.477	0.355	0.755	1.542	2.209	2.454	2.451
1.000	0.521	0.378	0.790	1.587	2.251	2.486	2.479
1.500	0.723	0.543	1.178	2.339	3.150	3.432	3.415
2.000	0.707	0.499	1.010	2.035	2.762	3.006	2.981
3.000	0.781	0.537	1.066	2.100	2.831	3.069	3.045
4.000	0.832	0.561	1.099	2.142	2.876	3.109	3.085
5.000	0.854	0.571	1.113	2.159	2.894	3.125	3.102
6.000	0.874	0.581	1.124	2.171	2.907	3.135	3.112
7.000	0.885	0.586	1.129	2.170	2.903	3.127	3.103
8.000	0.901	0.594	1.142	2.194	2.930	3.153	3.128
9.000	0.907	0.597	1.145	2.195	2.928	3.149	3.123
10.000	0.922	0.604	1.159	2.217	2.953	3.174	3.148
11.000	0.929	0.607	1.163	2.219	2.955	3.175	3.149
12.000	0.938	0.611	1.170	2.227	2.963	3.183	3.156
13.000	0.949	0.617	1.179	2.240	2.977	3.197	3.171
13.500	0.955	0.619	1.183	2.247	2.985	3.204	3.178

(This table is available in its entirety in the online journal, and at CDS in machine-readable format. Values for solar metallicity and helium content are shown here for guidance regarding its form and content.)

S-types of all the members, plus and minus the rms dispersion δ (log t) = 0.14 found by Girardi et al. (1995) for the log t – S relation.

Figure 6 shows five two-colour diagrams, comparing model SSPs with data of the superclusters, respectively $[V-I]$ vs. $[H-Ks]$, $[V-I]$ vs. $[J-Ks]$, $[V-Ks]$ vs. $[H-Ks]$, $[V-Ks]$ vs. $[J-Ks]$, and $[H-Ks]$ vs. $[J-H]$. Near-IR data have been taken from the Two Micron All Sky Survey (2MASS, Skrutskie et al. 1997); I-band data were retrieved from the Deep Near-Infrared Southern Sky Survey (DENIS; Epchtein et al. 1997); and V data come from different sources in the literature, mostly from the compilation by van den Bergh (1981, see González-Lópezlira et al. 2005). Near-IR colours for the superclusters were derived for the first time by González et al. (2004), $[V-I]$ by González-Lópezlira et al. (2005), and $[V-K_s]$ specifically for the present work. We have rederived $[V-I]$ and the near-IR colours, however, to make sure that the individual cluster centres are right, that both an image and stellar photometry are available for all clusters included in each supercluster, and that the background subtraction is optimal.[7] Whereas the near-IR colours were measured in the supercluster mosaics, using circular apertures with $r = 1'$, colours involving V ($[V-I]$, $[V-J]$, $[V-H]$, and $[V-K_s]$) were first obtained for single clusters, using the (diverse) diaphragms and V magnitudes from the compilation by van den Bergh (1981), and then averaged to derive colours for the superclusters. In these cases, the quoted errors equal the dispersion of the individual colours, divided by $(N-1)^{1/2}$, with N the number of objects in each supercluster. Measured colours for all superclusters are presented in Table 5, together with their ages, metallicities, and photometric masses. Except for supercluster SWB I, masses are always lower than estimated by González et al. (2004); for types III–VII, this is due more to our younger (on average, half as old) adopted ages than to changes between the BC03 (used by those authors) and the CB09 models. While the new assumed ages of types pre-SWB, I, and II are older (on average, twice as old), type I's estimated mass is the same and type II's, about 30% lighter. The only noteworthy case is the pre-SWB supercluster: its new estimated mass is only 10% of the one derived

---

[7] We have discovered, for example, that NGC 1854 and NGC 1855, both reportedly type SWB II, are actually the same cluster! Their putative centres are listed to be $6\farcs1$ apart; their respective S-parameters are, according to Elson & Fall (1985), 24 and 22, a difference that provides an independent estimate of the uncertainty in the assignment of S.

Table 2. Colours for CB09 models with fiducial mass-loss plus dusty envelopes

Age (Gyr)	$B-V$	$V-R$	$V-I$	$V-J$	$V-H$	$V-K_s$	$V-K$
$Z = 0.017$ $Y = 0.26$							
0.005	-0.142	-0.027	-0.043	-0.115	-0.031	-0.010	-0.017
0.006	-0.063	0.062	0.144	0.339	0.622	0.699	0.681
0.007	-0.059	0.070	0.175	0.443	0.793	0.900	0.878
0.008	-0.075	0.062	0.184	0.524	0.950	1.097	1.071
0.009	-0.133	0.020	0.161	0.604	1.146	1.354	1.324
0.010	-0.138	0.029	0.201	0.721	1.311	1.531	1.499
0.020	-0.071	0.096	0.348	0.967	1.606	1.816	1.781
0.030	-0.021	0.127	0.369	0.931	1.528	1.709	1.677
0.040	0.002	0.126	0.335	0.815	1.353	1.510	1.480
0.050	0.035	0.138	0.339	0.790	1.296	1.437	1.409
0.060	0.051	0.143	0.340	0.777	1.264	1.399	1.372
0.070	0.087	0.165	0.369	0.818	1.291	1.425	1.401
0.080	0.097	0.172	0.381	0.834	1.304	1.437	1.414
0.090	0.117	0.186	0.405	0.869	1.338	1.468	1.446
0.100	0.130	0.196	0.421	0.896	1.368	1.498	1.475
0.200	0.143	0.206	0.480	1.494	2.324	2.581	2.609
0.300	0.174	0.215	0.495	1.325	2.106	2.395	2.425
0.400	0.228	0.233	0.527	1.282	2.021	2.276	2.297
0.500	0.279	0.252	0.557	1.290	1.983	2.172	2.179
0.600	0.315	0.269	0.586	1.325	2.021	2.213	2.220
0.700	0.392	0.301	0.638	1.369	2.062	2.261	2.270
0.800	0.435	0.320	0.664	1.378	2.063	2.265	2.277
0.900	0.482	0.342	0.698	1.408	2.088	2.287	2.298
1.000	0.526	0.364	0.731	1.451	2.122	2.305	2.310
1.500	0.746	0.520	1.077	2.151	2.999	3.192	3.188
2.000	0.711	0.504	0.987	2.081	2.872	3.054	3.045
3.000	0.783	0.537	1.052	2.144	2.926	3.111	3.094
4.000	0.834	0.561	1.095	2.209	2.998	3.181	3.159
5.000	0.856	0.571	1.110	2.215	2.997	3.186	3.163
6.000	0.874	0.581	1.120	2.207	2.977	3.172	3.148
7.000	0.886	0.586	1.124	2.193	2.951	3.147	3.123
8.000	0.902	0.594	1.137	2.211	2.967	3.164	3.140
9.000	0.908	0.597	1.140	2.206	2.956	3.154	3.129
10.000	0.922	0.604	1.155	2.230	2.983	3.182	3.157
11.000	0.929	0.607	1.160	2.233	2.985	3.186	3.160
12.000	0.938	0.611	1.167	2.242	2.994	3.195	3.169
13.000	0.950	0.617	1.176	2.255	3.008	3.210	3.184
13.500	0.955	0.619	1.181	2.261	3.014	3.217	3.191

(This table is available in its entirety in the online journal, and at CDS in machine-readable format. Values for solar metallicity and helium content are shown here for guidance regarding its form and content.)

by González et al. (2004), and hence its SBF amplitudes are shown now with significantly larger uncertainties.

In all the panels, the data (solid black circles with error bars) are compared to models with a fiducial mass-loss rate and 3 different metallicities ($Z = 0.0004$, blue; 0.008, cyan; 0.017, red), that bracket those of the superclusters ($0.0007 \leqslant Z \leqslant = 0.01$; Frogel et al. 1990, assuming that $Z_\odot = 0.017$; Cohen 1982). The expected $\pm 1\sigma$ error bars for the models, shown as coloured bands, have been calculated as in González et al. (2004, Appendix), assuming a stellar population of 5×10^5 $M_\odot$. This value is conservative, and representative of the MC superclusters; they have between $\sim 10^5$ and $\sim 3 \times 10^6$ $M_\odot$. The two superclusters where the effects of AGB stars should be more important (aged 160 and 450 Myr, respectively) have both $\sim 5 \times 10^5$ $M_\odot$ in stars. Roughly, the models have no problem explaining the colours of the superclusters, although we notice that the pre-SWB supercluster lies quite far away from the models in the bottom left panel of the figure ($[H - K_s]$ vs. $[J - H]$). We hypothesise that this supercluster might suffer from additional extinction (see González-Lópezlira et al. 2005) and systematic effects. Firstly, in the optical and even in the near-IR, there might be a selection against very young clusters that are the product of the most energetic star formation. In fact, although 2MASS data for NGC 2070 (30 Dor) were available, they were not used to build the supercluster type pre-SWB because they showed abundant nebular emission and dust extinction. Also, regarding very young clusters, the assumption that the addition of many small objects is statistically equal to a large one will fail, if none of the small clusters is massive enough to produce the most massive stars. This problem is not relevant after a few 10^7 yr, when these stars die and cease to contribute to the cluster's light.

Perhaps more useful to assess the models is the comparison with the data in the age–colour planes. Figure 7 shows the data compared to colour versus age for models with a fiducial mass-loss rate. The trends of colour with age shown by the data are very closely followed by the models.

It is also instructive to compare our models to the cluster sample already compiled and presented by Piovan et al. (2003).[8] Once again, two-colour diagrams are shown in Fig. 8: $[V - K]$ vs. $[H - K]$; $[V - K]$ vs. $[J - K]$; and $[H - K]$ vs. $[J - H]$. The data are clusters mostly younger than 1.5 Gyr, and are displayed as filled circles, with average error bars shown for each panel. The expected $\pm 1\sigma$ error bars for the models are depicted once more as coloured regions, ex-

---

[8] The data were extracted by us from Piovan et al.'s paper with Dexter (Demleitner et al. 2001).

Table 3. SBF amplitudes for CB09 models with fiducial mass-loss but without dusty envelopes

Age (Gyr)	$\bar{M}_B$	$\bar{M}_V$	$\bar{M}_R$	$\bar{M}_I$	$\bar{M}_J$	$\bar{M}_H$	$\bar{M}_{K_s}$	$\bar{M}_K$
				$Z = 0.017 \quad Y = 0.26$				
0.005	-7.637	-7.809	-8.061	-8.340	-8.999	-9.510	-9.644	-9.617
0.006	-7.446	-7.697	-8.168	-8.678	-9.705	-10.389	-10.559	-10.521
0.007	-7.171	-7.415	-7.887	-8.432	-9.546	-10.286	-10.487	-10.446
0.008	-6.885	-7.052	-7.457	-8.033	-9.295	-10.137	-10.390	-10.347
0.009	-6.427	-6.470	-6.701	-7.330	-8.979	-9.998	-10.330	-10.286
0.010	-6.096	-6.092	-6.352	-7.155	-8.963	-9.984	-10.313	-10.270
0.020	-4.936	-4.972	-5.263	-6.051	-7.692	-8.698	-8.999	-8.954
0.030	-4.390	-4.500	-4.818	-5.491	-6.951	-7.945	-8.232	-8.186
0.040	-3.884	-4.049	-4.370	-4.973	-6.338	-7.338	-7.621	-7.573
0.050	-3.382	-3.658	-4.031	-4.624	-5.937	-6.929	-7.205	-7.156
0.060	-2.990	-3.367	-3.795	-4.406	-5.737	-6.742	-7.027	-6.977
0.070	-2.251	-2.832	-3.385	-4.052	-5.581	-6.665	-7.028	-6.975
0.080	-1.895	-2.547	-3.172	-3.883	-5.510	-6.626	-7.017	-6.964
0.090	-1.629	-2.341	-3.019	-3.754	-5.397	-6.517	-6.914	-6.860
0.100	-1.326	-2.066	-2.799	-3.577	-5.291	-6.428	-6.837	-6.782
0.200	-0.291	-0.671	-1.485	-3.217	-6.837	-8.026	-8.527	-8.478
0.300	0.083	-0.254	-1.139	-2.915	-6.166	-7.531	-8.121	-8.157
0.400	0.508	0.117	-0.786	-2.666	-5.760	-7.132	-7.724	-7.766
0.500	0.812	0.339	-0.595	-2.622	-5.698	-6.981	-7.496	-7.492
0.600	0.992	0.435	-0.555	-2.597	-5.600	-6.887	-7.406	-7.410
0.700	1.364	0.619	-0.483	-2.525	-5.359	-6.664	-7.198	-7.221
0.800	1.552	0.694	-0.461	-2.473	-5.199	-6.523	-7.072	-7.109
0.900	1.721	0.744	-0.447	-2.419	-5.072	-6.405	-6.967	-7.012
1.000	1.890	0.805	-0.405	-2.337	-4.968	-6.300	-6.869	-6.912
1.500	1.985	0.421	-0.890	-2.793	-5.305	-6.491	-7.032	-7.072
2.000	2.420	0.991	-0.160	-1.837	-4.897	-6.073	-6.568	-6.535
3.000	2.632	1.171	0.045	-1.563	-4.603	-5.795	-6.317	-6.305
4.000	2.893	1.321	0.201	-1.360	-4.433	-5.640	-6.174	-6.169
5.000	2.948	1.411	0.307	-1.218	-4.285	-5.499	-6.034	-6.032
6.000	2.513	1.413	0.384	-1.076	-4.138	-5.358	-5.885	-5.880
7.000	2.745	1.540	0.490	-0.958	-4.036	-5.262	-5.785	-5.773
8.000	2.694	1.554	0.519	-0.912	-4.025	-5.248	-5.765	-5.744
9.000	2.844	1.635	0.593	-0.838	-3.995	-5.220	-5.734	-5.705
10.000	2.786	1.640	0.611	-0.815	-3.960	-5.181	-5.692	-5.663
11.000	2.783	1.685	0.664	-0.767	-3.917	-5.139	-5.650	-5.620
12.000	2.716	1.703	0.696	-0.732	-3.880	-5.102	-5.613	-5.582
13.000	2.818	1.744	0.729	-0.704	-3.856	-5.077	-5.587	-5.556
13.500	2.788	1.743	0.734	-0.695	-3.846	-5.066	-5.576	-5.545

(This table is available in its entirety in the online journal, and at CDS in machine-readable format. Values for solar metallicity and helium content are shown here for guidance regarding its form and content.)

cept that now we are assuming a population of $10^5\ M_\odot$. The models have a fiducial mass-loss rate; and metallicities $Z = 0.008$ (*cyan*) and $Z = 0.017$ (*red*), that encompass those of the clusters. Model ages go from 100 Myr to 1.5 Gyr.

The match is comparable to that achieved by Piovan et al. (2003, their Figure 16) for most colours, and considerably better for $[V - K]$ vs. $[H - K]$, even though our model ages in the figure stop at 1.5 Gyr (theirs go up to 15 Gyr).

We have seen so far that our models are able to fit both near-IR colours of most single AGB stars, and integrated optical and near-IR colours of star clusters with different ages and metallicities. Integrated colours of star clusters, however, do not seem to be able to discriminate between different choices of global mass-loss rates. Next, we will investigate whether surface brightness fluctuations are potentially sensitive to different mass-loss rates in stellar populations.

4 SURFACE BRIGHTNESS FLUCTUATIONS, METALLICITY, AND MASS-LOSS.

The technique of surface brightness fluctuation (SBF) measurements was introduced by Tonry & Schneider (1988) as a way to derive distances to early-type galaxies. The fluctuation flux (denoted $\bar{f}$) is the ratio between the variance and the mean of the stellar luminosity function (Tonry & Schneider 1988; Tonry et al. 1990), scaled by $(4\pi d^2)^{-1}$, where d is the distance. This is expressed as follows:

$$\bar{f} = \frac{1}{4\pi d^2} \frac{\Sigma n_i l_i^2}{\Sigma n_i l_i}; \tag{1}$$

n_i and l_i are, respectively, the number of stars of type i, and their luminosity.

In the case of galaxies, the fluctuation magnitude[9] $\bar{m}$ is measured through the spatial fluctuations in their surface brightness, and the distance is found by comparing $\bar{m}$ with empirically calibrated relations that give the absolute fluctuation magnitude, $\bar{M}$, in a photometric band as a function of a certain broadband colour, in a given range (e.g., Worthey 1993a,b; Pahre & Mould 1994; Tonry et al. 1997; Ajhar et al. 1997; Liu et al. 2000, 2002; Mei et al. 2001; Jensen et al. 2003; Cantiello et al. 2003, 2005; Mei et al. 2005a,b; González-Lópezlira et al. 2005; Marín-Franch & Aparicio 2006; Mei et al. 2007; Cantiello et al. 2007a,b; Blakeslee et al. 2009). In nearby stellar clusters, it is possible to obtain $\bar{m}$ by performing the sums in equation 1 over resolved stars (Ajhar & Tonry

---

[9] $\bar{m} = -2.5 \log \bar{f} +$ zero point.

Table 4. SBF amplitudes for CB09 models with fiducial mass-loss plus dusty envelopes

Age (Gyr)	$\bar{M}_B$	$\bar{M}_V$	$\bar{M}_R$	$\bar{M}_I$	$\bar{M}_J$	$\bar{M}_H$	$\bar{M}_{K_s}$	$\bar{M}_K$
				$Z = 0.017 \quad Y = 0.26$				
0.005	-7.637	-7.809	-8.061	-8.340	-8.999	-9.510	-9.644	-9.617
0.006	-7.446	-7.697	-8.168	-8.678	-9.705	-10.389	-10.559	-10.521
0.007	-7.171	-7.415	-7.887	-8.432	-9.546	-10.286	-10.487	-10.446
0.008	-6.885	-7.052	-7.457	-8.033	-9.295	-10.137	-10.390	-10.347
0.009	-6.427	-6.470	-6.701	-7.330	-8.979	-9.998	-10.330	-10.286
0.010	-6.096	-6.092	-6.352	-7.155	-8.963	-9.984	-10.313	-10.270
0.020	-4.936	-4.972	-5.263	-6.051	-7.692	-8.698	-8.999	-8.954
0.030	-4.390	-4.500	-4.818	-5.491	-6.951	-7.945	-8.232	-8.186
0.040	-3.884	-4.049	-4.370	-4.973	-6.338	-7.338	-7.621	-7.573
0.050	-3.382	-3.658	-4.031	-4.624	-5.937	-6.929	-7.205	-7.156
0.060	-2.990	-3.367	-3.795	-4.406	-5.737	-6.742	-7.027	-6.977
0.070	-2.251	-2.832	-3.385	-4.052	-5.581	-6.665	-7.028	-6.975
0.080	-1.895	-2.547	-3.172	-3.883	-5.510	-6.626	-7.017	-6.964
0.090	-1.629	-2.341	-3.019	-3.754	-5.397	-6.517	-6.914	-6.860
0.100	-1.326	-2.066	-2.799	-3.577	-5.291	-6.428	-6.837	-6.782
0.200	-0.291	-0.679	-1.538	-2.995	-7.066	-8.424	-8.685	-8.739
0.300	0.084	-0.265	-1.170	-2.763	-6.233	-7.724	-8.144	-8.223
0.400	0.510	0.093	-0.805	-2.477	-5.646	-7.198	-7.676	-7.766
0.500	0.816	0.310	-0.584	-2.277	-5.443	-6.961	-7.349	-7.421
0.600	0.999	0.410	-0.517	-2.208	-5.324	-6.852	-7.265	-7.341
0.700	1.382	0.623	-0.360	-2.024	-5.028	-6.603	-7.089	-7.179
0.800	1.582	0.727	-0.274	-1.898	-4.839	-6.457	-6.997	-7.096
0.900	1.765	0.802	-0.216	-1.800	-4.702	-6.346	-6.913	-7.013
1.000	1.949	0.876	-0.152	-1.708	-4.601	-6.245	-6.801	-6.890
1.500	2.091	0.443	-0.750	-2.336	-4.957	-6.392	-6.875	-6.950
2.000	2.426	0.986	-0.211	-1.620	-5.062	-6.408	-6.671	-6.702
3.000	2.635	1.169	0.033	-1.428	-4.818	-6.175	-6.445	-6.459
4.000	2.895	1.319	0.197	-1.326	-4.841	-6.219	-6.460	-6.454
5.000	2.950	1.410	0.306	-1.186	-4.658	-6.035	-6.300	-6.292
6.000	2.513	1.413	0.384	-1.040	-4.393	-5.754	-6.056	-6.047
7.000	2.745	1.540	0.491	-0.920	-4.204	-5.548	-5.882	-5.870
8.000	2.694	1.554	0.519	-0.875	-4.145	-5.473	-5.816	-5.802
9.000	2.844	1.635	0.593	-0.804	-4.081	-5.400	-5.755	-5.735
10.000	2.786	1.640	0.611	-0.784	-4.057	-5.369	-5.730	-5.708
11.000	2.783	1.685	0.664	-0.738	-4.022	-5.333	-5.701	-5.677
12.000	2.716	1.703	0.697	-0.706	-3.992	-5.300	-5.676	-5.650
13.000	2.818	1.744	0.729	-0.681	-3.970	-5.274	-5.656	-5.630
13.500	2.788	1.743	0.734	-0.672	-3.958	-5.258	-5.645	-5.618

(This table is available in its entirety in the online journal, and at CDS in machine-readable format. Values for solar metallicity and helium content are shown here for guidance regarding its form and content.)

1994; González et al. 2004; González-Lópezlira et al. 2005; Mouhcine et al. 2005; Raimondo et al. 2005).

It is not hard to see that SBFs convey information about stellar populations, akin to integrated photometry and spectra. However, because of their dependence on the square of the stellar luminosity, they are especially sensitive to, and can provide additional information about the brightest stars at a particular wavelength and at a given evolutionary phase of a stellar population. Accordingly, it has been suggested recently (Cantiello et al. 2003; Raimondo et al. 2005, González-Lópezlira & Buzzoni 2008) that SBFs can be used to study AGB stars in intermediate-age populations and, specifically, to investigate their mass-loss rates. These works, though, do not explore a possible intrinsic connection between metallicity and mass-loss, nor consider the impact of extinction by dust in the stellar envelope on the detectability of mass-losing stars.

Surprisingly in a way, the relation between metallicity and mass-loss turns out to be controversial, even for the dust-driven winds in the TP-AGB. On the one hand, detailed theoretical models (e.g. Willson 2000) predict that mass-loss should increase with metallicity, and Groenewegen et al. (1995) have found, from fits to $8-13\mu$m spectra, mass-loss rate ratios of 4:3:1 for three O-rich AGB stars with similar periods in, respectively, our Galaxy, the LMC, and the Small Magellanic Cloud (SMC).[10] More recently, Kalirai et al. (2005, 2008) have found evidence of a metallicity dependence of the initial-final mass relationship (between the mass of a white dwarf remnant and its main-sequence predecessor) from spectroscopic observations of white dwarfs in open clusters. On the other hand, Gail & Sedlmayr (1986) propose that the mass-loss rate is proportional to the ratio $\tau/v_{\rm exp}$, where τ is the optical depth of a dust-driven wind and $v_{\rm exp}$ is its velocity. Van Loon (2000) derives a metallicity-independent mass-loss rate for a sample of dust-obscured C and O-rich AGB stars, also in the Milky Way, the LMC, and the SMC. Correspondingly, van Loon (2006) argues that both τ and $v_{\rm exp}$ depend on the square root of the dust-to-gas ratio, Ψ, that presumably is itself linearly proportional to metallicity, such that the dependence of $\dot{M}$ on Z cancels out. Today, however, we know that Ψ is not constant with metallicity, and that both the dust-to-gas ratio and the dust species in the stellar envelopes vary during evolution for a single star and between

---

[10] The present-day [Fe/H] ratios for the Sun, and B-type stars in the LMC and the SMC are $\sim$ 3:2:1 (Mokiem et al. 2007); according to Lyubimkov et al. (2005), the Sun and B-type MS stars in the solar neighbourhood have the same metallicity. The ratios for the Sun and F-type stars are $\sim$ 4:2:1 (Russell & Bessell 1989).

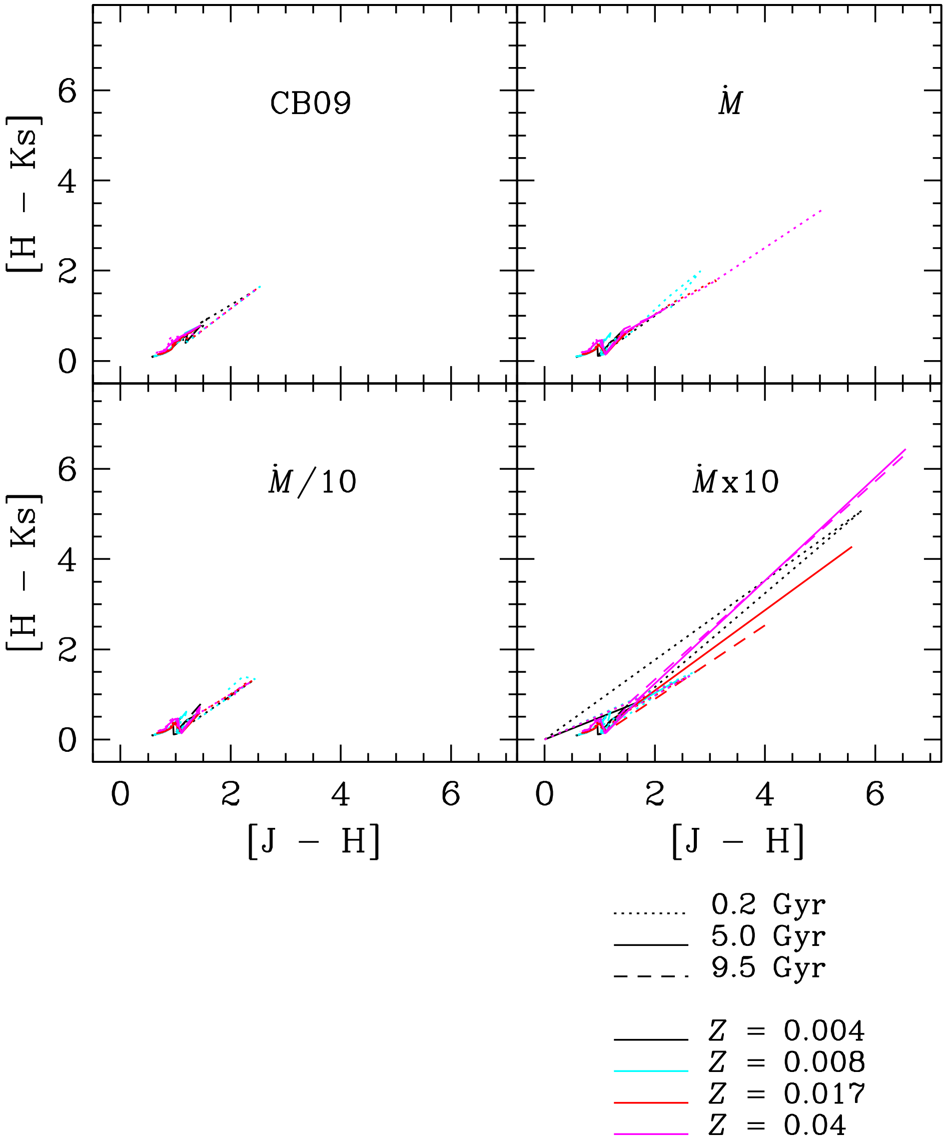

Figure 1. Theoretical two-colour diagrams, $[H - K_s]$ vs. $[J - H]$, of individual stars along the 0.2 Gyr (*dotted line*), 5.0 Gyr (*solid line*), and 9.5 Gyr (*dashed line*) isochrones, for populations with different mass-loss rates and metallicities. *Top left:* standard CB09; *bottom left:* fiducial $\dot{M}/10$; *top right:* fiducial $\dot{M}$; *bottom right:* fiducial $\dot{M} \times 10$. Different colours indicate diverse metallicities, i.e., *black:* $Z = 0.004$; *cyan:* $Z = 0.008$; *red:* $Z = 0.017$; *magenta:* $Z = 0.04$.

different stars with the same initial metallicity (see, e.g., Lebzelter et al. 2006; Ferrarotti & Gail 2006).

With the aim of addressing the question of the relation between Z and $\dot{M}$, we compute the time evolution of SBF magnitudes of single-burst stellar populations in the B, V, R, I, J, H, and K_S bands, in the nine metallicities and helium contents mentioned before. The model fluctuation luminosity $\bar{L}$ at each wavelength is calculated with the following equation (very similar to eq. 1):

$$\bar{L} = \frac{\Sigma w_i l_i^2}{\Sigma w_i l_i}, \tag{2}$$

where the weight w_i is the number of stars of type i *per unit mass* in the population (set as explained in Section A1), and l_i is the luminosity of stellar type i.[11]

Following Cerviño et al. (2002), González et al. (2004) demonstrated that the theoretical relative errors of fluctuation magnitudes and colours also scale as $M_{\rm tot}^{-1/2}$, if a Poissonian distribution is assumed for the stellar numbers in different evolutionary phases. In the rest of this paper, we show calculations for stellar populations with $5 \times 10^5 M_\odot$; this number is representative of the MC "superclusters".

---

[11] The corrected stellar weights were, of course, also applied to the calculation of integrated colours used in Section 3.

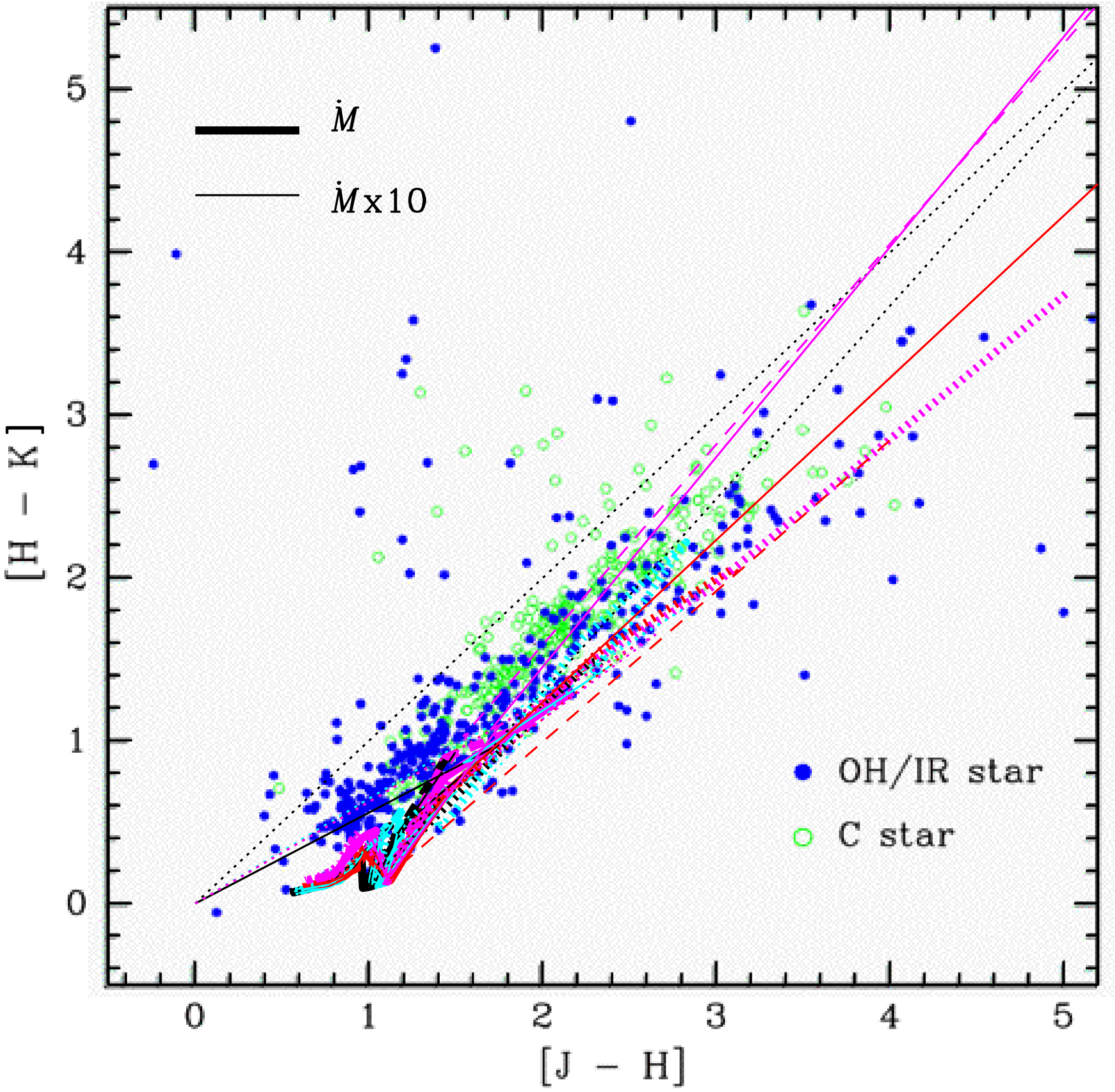

Figure 2. $[H-K]$ vs. $[J-H]$ integrated colours of individual OH/IR and Mira stars from various sources in the literature. *Blue solid circles:* O-rich stars; *green open circles:* C-stars. The data were originally compiled and properly corrected for extinction by Piovan et al. (2003). J, H, and K magnitudes brighter than 7 have typical uncertainties of 0.05 mag. Theoretical colours of individual stars are superimposed on the sample of observed AGB stars. *Thick* lines: fiducial mass-loss rate $\dot{M}$; *thin* lines: high mass-loss rate $\dot{M}\times$ 10. Metallicity and age symbols as in Fig. 1.

5 SBF RESULTS.

5.1 Model SBFs.

Figure 9 shows absolute fluctuation magnitudes vs. log (age) for standard CB09 models with different metallicities, from $Z = 0.0004$ ($\sim 1/40$ solar) to $Z = 0.07$ (~ 4 times solar). Coloured regions delimit expected $\pm\,1\,\sigma$ stochastic errors for a stellar population with $5\times10^5\ M_\odot$. In the optical bands (B to I), SBFs grow systematically fainter as metallicity increases. The reason is that the brightest stars (those that dominate the SBF signal) will be cooler (redder) at higher metallicities. Another consequence of the same phenomenon is that errors grow notably larger with metallicity in B and V for ages greater than a few Gyr; a higher metallicity translates into fewer hot and blue stars, implying larger stochastic errors. A very similar trend with metallicity is seen for all the mass-loss rates explored in this paper.

The main difference with metallicity in the near-IR happens at very young ages ($\sim 10^7$ yr), between the most metal poor models ($Z = 0.0004$), and the rest. Metal poor populations will produce SBFs about 2 mag fainter in the near-IR at these ages, as a consequence of having fewer red supergiants; for the same reason, the stochastic error is largest ($\sim\pm1$ mag) for these metallicities and ages. Although it is strictly true that SBFs increase with metallicity in the J H, and K_s bands for populations $\sim 100-300$ Myr old, the sensitivity to Z is smaller at $1-2\mu$m. This is because, once the RGB is born, it is the most important contributor to the integrated light of stellar populations at these wavelengths (see, e.g., González et al. 2004); the variance (i.e., the SBFs) produced by the brightest red stars (both in the RGB and AGB) against this already bright background will then be less prominent. The onset of the TP-AGB is clearly discernible as a peak at about 10^8 years.

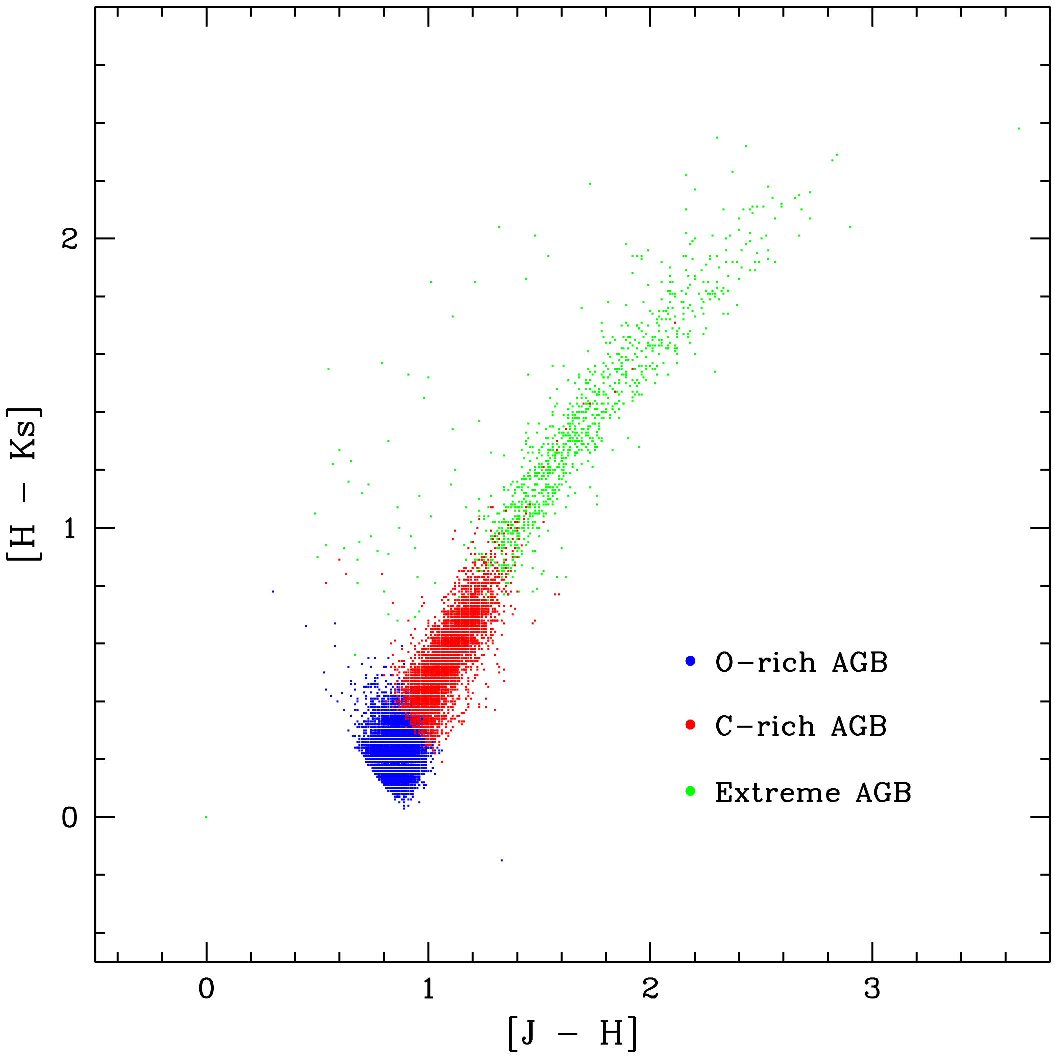

Figure 3. 2MASS $[H-K_s]$ vs. $[J-H]$ integrated colours of individual AGB candidates in the sample of Srinivasan et al. (2009). *Blue:* O-rich stars. *Red:* C-rich stars. *Green:* "extreme" AGB stars; these are the most luminous AGB stars, losing the most mass. Typical photometric errors are 0.05 mag for sources with $K_s \sim 11$ mag.

Figure 10 displays absolute fluctuation magnitudes vs. log (age) for models with $Z = 0.008$ and different mass-loss rates. This metallicity ($Z_\odot/2.1$) is closest to that of the youngest half of the MC star clusters whose data are presented below. Coloured regions delimit expected $\pm 1\sigma$ stochastic errors for a stellar population with $5 \times 10^5 M_\odot$. Contrary to the results of Raimondo et al. (2005), we find no strong trend of SBF brightness with mass-loss rate. The biggest difference is between the CB09 models without dusty envelopes and the models with dusty cocoons, regardless of $\dot{M}$. This difference is most noticeable in the I-band, where models with dust are about 0.5 mag fainter than CB09 standard models at all ages after 10^8 yr. The dusty models basically all fall on top of each other. Other metallicities show exactly the same behavior, with the exceptions of (1) the already pointed out lower brightness and larger dispersion of SBFs values for $Z = 0.0004$ and $Z = 0.001$ at 10^7 yr, and (2) a large scatter for the higher metallicities ($Z = 0.017$ to $Z = 0.07$) at ages greater than ~ 2 Gyr, in the B, V, and R passbands. In the latter case, the dispersion is caused by the lower emission from red giants in these bands; it increases with metallicity and decreases with wavelength, and goes from $\sim \pm 0.5$ mag, for $Z = 0.017$ at V, to $\sim \pm 4$ mag for $Z = 0.07$ at B.

The reason for this degeneracy is that the selection effects highlighted by Willson (2000) are intensified by extinction, and further exacerbated when the mass-loss rate is changed. The probability of detecting the effects of stars shedding their envelopes in an exponential fashion, already low owing to the short duration of the phase, will decrease if the stars are heavily dust-enshrouded. If the mass-loss-rate is modified upward, the intrinsic luminosity of stars in the superwind stages will increase, but their lifetimes in the phase will hence be even shorter and they will be more ob-

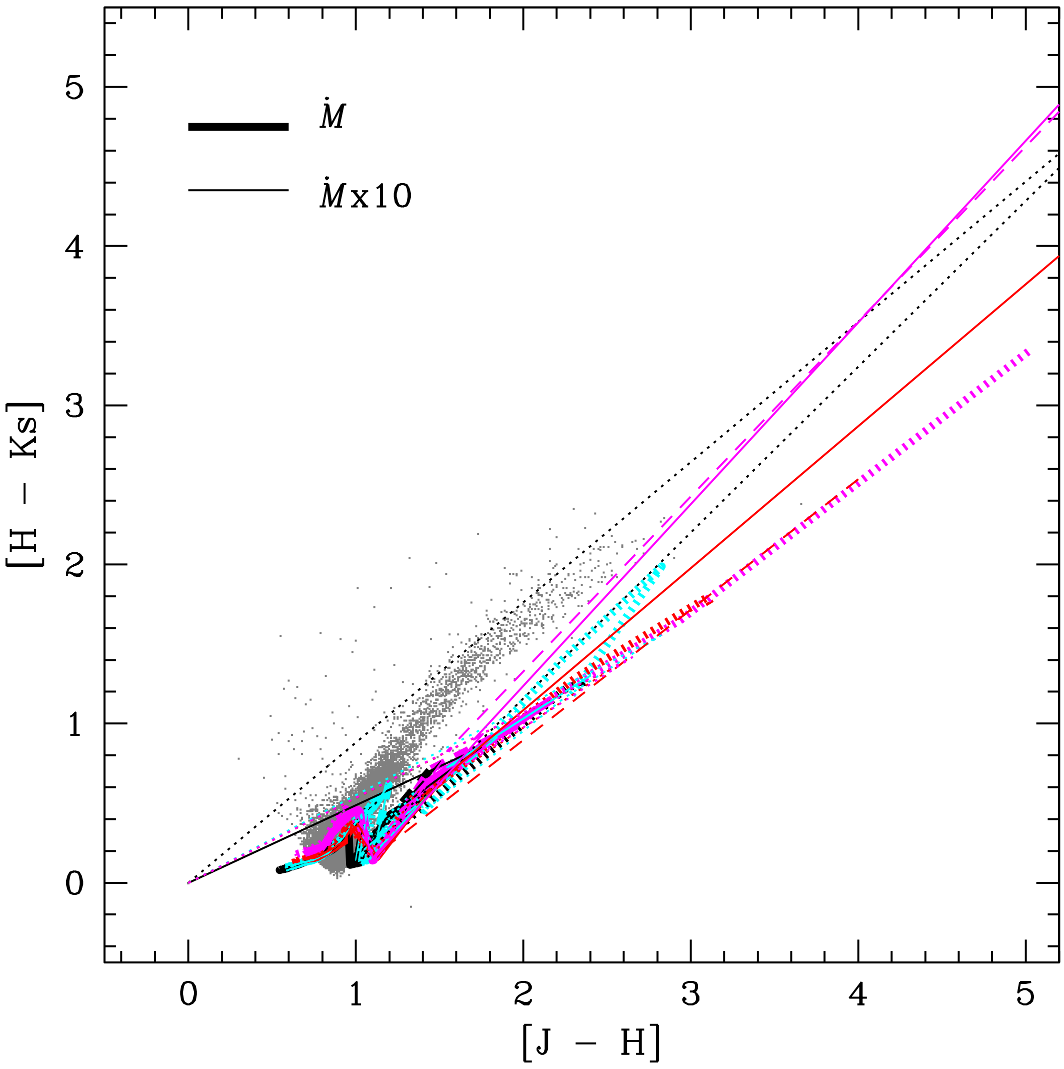

Figure 4. Theoretical colours of individual stars are superimposed on the sample of observed AGB stars, now shown as gray points. *Thick* lines: fiducial mass-loss rate $\dot{M}$; *thin* lines: high mass-loss rate $\dot{M}\times$ 10. Metallicity and age symbols as in Fig. 1.

scured. The stars losing the most mass sometimes will not survive past the first or second superwind stages. Contrariwise, if mass-loss rate is changed downward, stars will last longer and be less obscured, but their luminosity will go correspondingly down.

5.2 SBF data.

SBF magnitudes of MC star clusters have been determined previously by González et al. (2004, 2005) in the near-IR, and by Raimondo et al. (2005) in the optical. As discussed earlier, the former built 8 artificial "superclusters", whereas the latter chose to analyse Wide Field Planetary Camera 2 (WFPC2) Hubble Space Telescope (*HST*) V and I data of a dozen populous MC globular clusters.

González et al. derived SBFs for the "superclusters" within a radius of $1'$, as prescribed by equation 1. The numerator was found by summing the square of the flux of resolved, bright stars, obtained from the 2MASS Point Source Catalog; field contamination was minimized by excluding from the analysis stars in the range $12.3 < (K_s)_o < 14.3$ with colours $(J-K_s)_o > 1.2$ or $(J-K_s)_o < 0.4$ (Ferraro et al. 1995). Since the sum in the denominator converges slowly, it was computed from the total light detected in the images, after removal of the emission in an annulus with $2\farcm0 < r \leqslant 2\farcm5$; this was assumed to include the contributions from both sky and field stars. Absolute fluctuation magnitudes were assigned taking an LMC distance modulus $(m-M)_0 = 18.5$ (Ferrarese et al. 2000).

As it turns out, the colour function used by González et al. (2004) to select cluster stars is adequate for older clusters, but is too red for the 2 or 3 youngest superclusters. For this reason, we have recalculated near-IR fluctuation values for all the superclusters. This time, we have statistically removed the field population as per the procedure described by Mighell et al. (1996). We com-

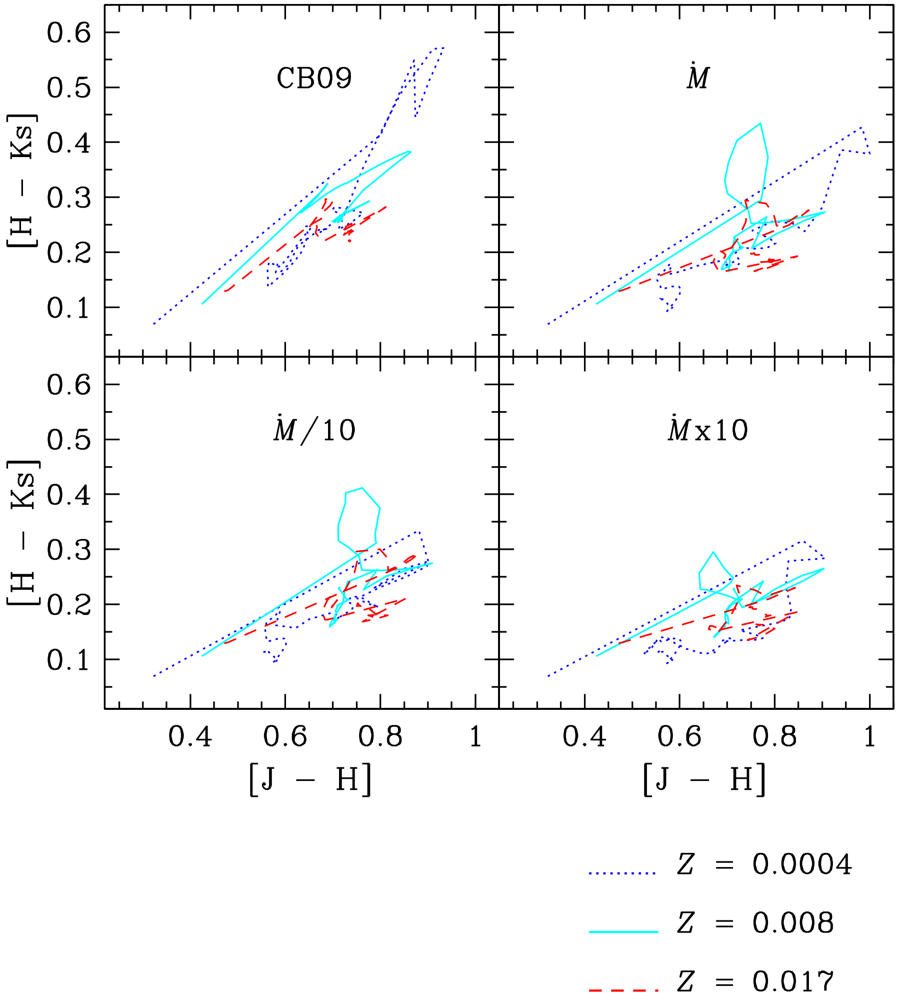

Figure 5. Theoretical two-colour diagrams, $[H - K_s]$ vs. $[J - H]$, for SSPs with different metallicities and mass-loss rates. *Top left:* standard CB09; *bottom left:* fiducial $\dot{M}/10$; *top right:* fiducial $\dot{M}$; *bottom right:* fiducial $\dot{M} \times 10$. Models span an age range between 100 Myr and 14 Gyr. *Blue:* $Z = 0.0004$; *cyan:* $Z = 0.008$; *red:* $Z = 0.017$.

pare, for each supercluster, the $[J - K_s]$ versus K_s diagram of stars within $r = 1'$ of the supercluster centre (i.e., the "cluster region"), with that of stars in an annulus with $2\farcm0 < r \leqslant 2\farcm5$ (i.e., the "field"); the former colour-magnitude diagram (CMD) presumably includes both cluster and field stars, whereas we assume that the latter contains only field stars. For each star in the cluster region with mag $Ks \pm \sigma_{Ks}$ and colour $[J - K_s]$ $\pm\sigma_{[J-Ks]}$, we count the number of stars in the same CMD with $[J - K_s]$ colours within $\pm$MAX($2\sigma_{[J-Ks]}$,0.100) mag and K_s mag within $\pm$MAX($2\sigma_{Ks}$,0.200) mag. We call this number $N_{\rm scl}$. We also count the number of stars in the field CMD within the same ΔK_s by Δ $[J - K_s]$ bin determined from the cluster star. We call this number $N_{\rm fld}$. The probability p that the star in the cluster region CMD actually belongs to the supercluster can be expressed as:

$$p \approx 1 - \mathrm{MIN}\left(\frac{\alpha(N_{\rm fld}+1)}{N_{\rm scl}+1}, 1.0\right), \qquad (3)$$

where α, in this case 0.44, is the ratio of the area of the cluster region (π arcmin^2) to the area of the field region (2.25 π arcmin^2). Once p is calculated for a given star, it is compared to a randomly drawn number $0 \leqslant p' \leqslant 1$. If $p \geqslant p'$, the star is accepted as a supercluster member; otherwise, it is rejected and considered as a field object.

The numerator of equation 1 was calculated with the decontaminated star lists. We have obtained the denominator in the same way as before, i.e., from the total light within

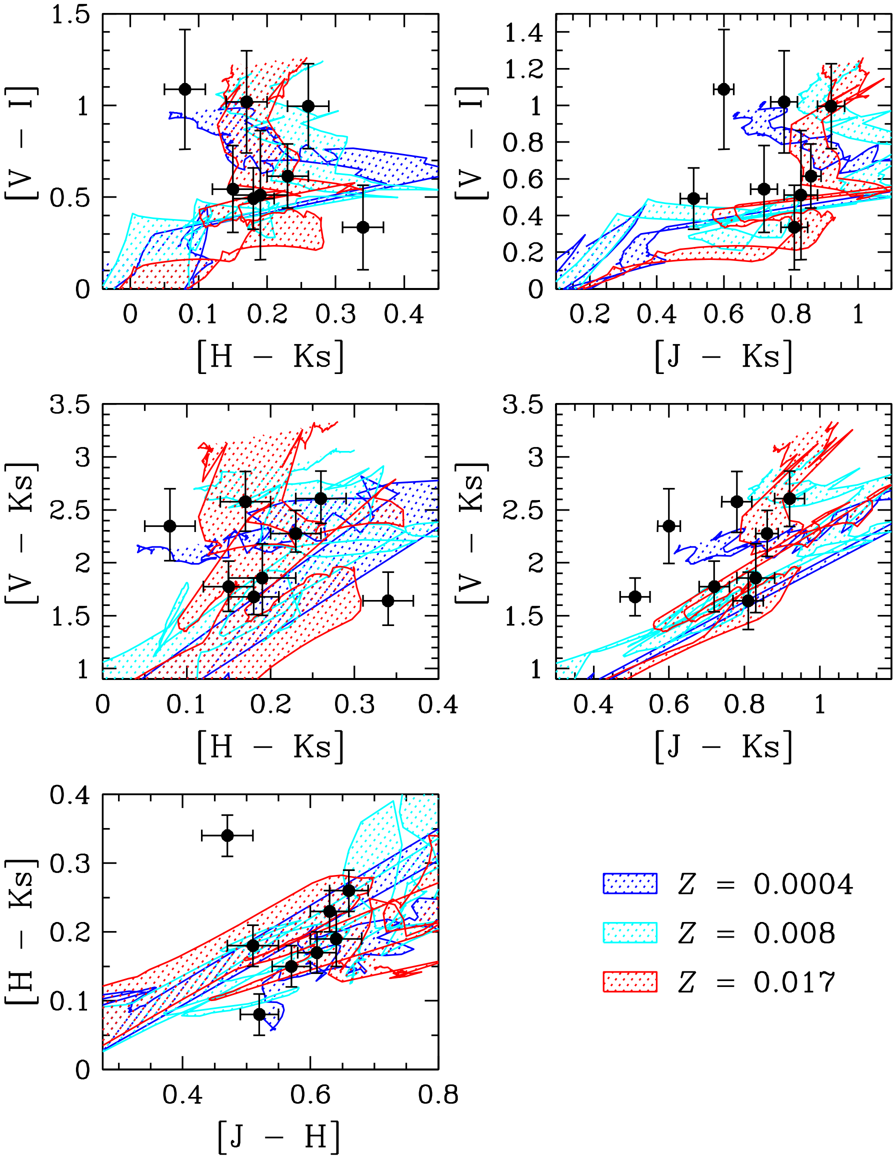

Figure 6. Comparison between models and MC "superclusters": two-colour diagrams. *Top left:* $[V-I]$ vs. $[H-K_s]$; *top right:* $[V-I]$ vs. $[J-K_s]$; *middle left:* $[V-K_s]$ vs. $[H-K_s]$; *middle right:* $[V-K_s]$ vs. $[J-K_s]$; *bottom left:* $[H-K_s]$ vs. $[J-H]$. Filled circles are artificial "superclusters" built by González et al. (2004, 2005); González-Lópezlira et al. (2005). Coloured regions represent SSPs with fiducial $\dot{M}$ and expected $\pm 1\sigma$ error bars for $5{\times}10^5\ M_{\odot}$. *Blue:* $Z = 0.0004$; *cyan:* $Z = 0.008$; *red:* $Z = 0.017$. Supercluster ages go from 6 Myr to 10 Gyr; model ages span between 3 Myr and 14 Gyr.

$r = 1'$, after subtracting the light in the annulus between $2\overset{'}{.}0$ and $2\overset{'}{.}5$. The new SBF values tend to be fainter than the González et al. (2004) ones; both sets of values agree within 1 σ, though, with the exception of the SWB I supercluster, whose SBF determinations coincide within 3 σ.[12]

We have also derived $\bar{M}_I$ for the eight superclusters using DENIS images, and photometry of the point sources from the DENIS database[13] and the DENIS Point Source Catalogue towards the Magellanic Clouds (Cioni et al. 2000). The procedure is the same as for near-IR fluctuation magnitudes, except that $[I-J]$ versus I diagrams have been

---

[12] An alternative approach for the decontamination, using the field CMD as the reference (i.e., "field" stars are removed from the cluster region, rather than "cluster" stars kept), has been used and described by Gallart et al. (2003). We have tried this method, and obtain the same results. We have also tried using the annulus with $2\overset{'}{.}5 < r \leqslant 3\overset{'}{.}0$ as the "field". Once again, the results do not vary significantly, except for the pre-SWB supercluster, although even in this case both new derived sets of SBF values lie within the (considerably large) errors.

[13] Third release of DENIS data, The DENIS Consortium, 2005; http://cdsarc.u-strasbg.fr/viz-bin/Cat?B/denis.

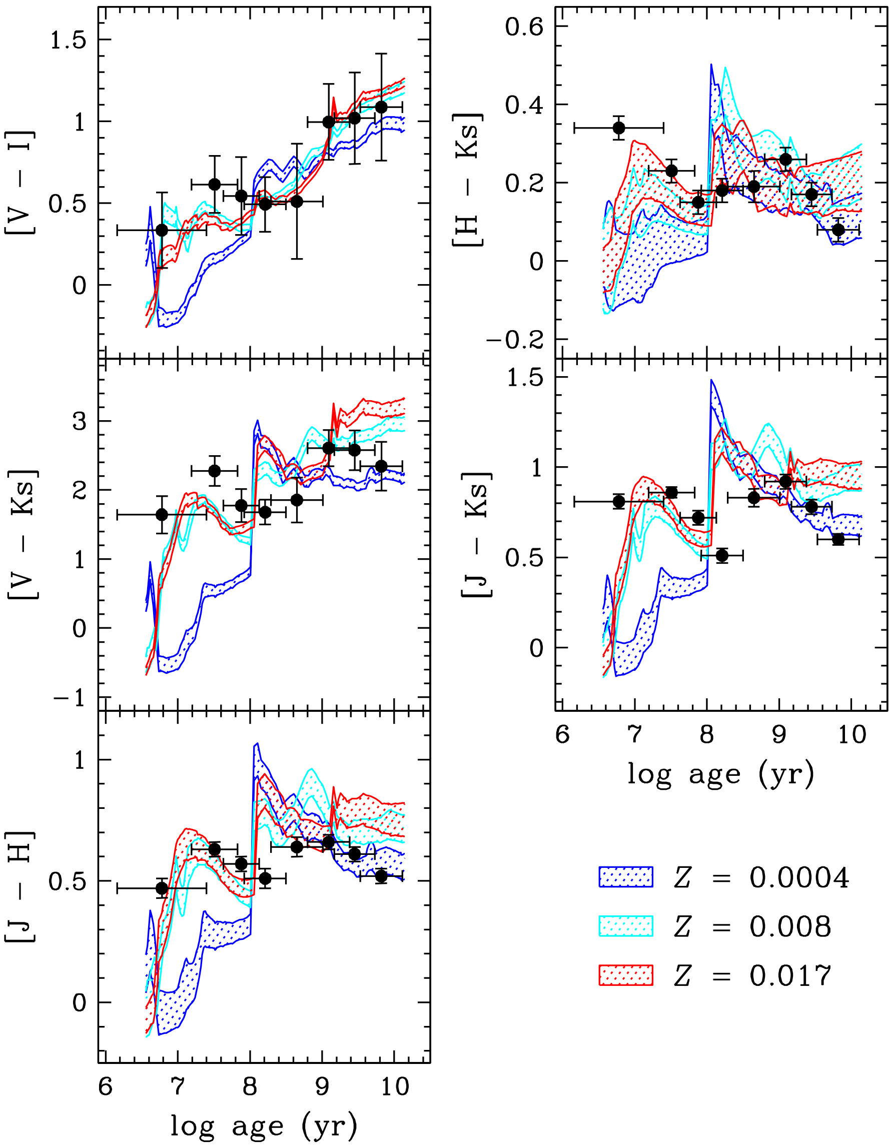

Figure 7. Comparison between models and MC "superclusters": colours vs. log (age). *Top left:* $[V-I]$; *middle left:* $[V-K_s]$; *bottom left:* $[J-H]$; *top right:* $[H-K_s]$; *middle right:* $[J-K_s]$. Coloured regions represent SSPs with fiducial $\dot{M}$ and expected $\pm1\sigma$ error bars for $5{\times}10^5$ $M_\odot$, coded as in Figure 6.

employed for the field decontamination. SBF measurements for the superclusters are provided in Table 5.

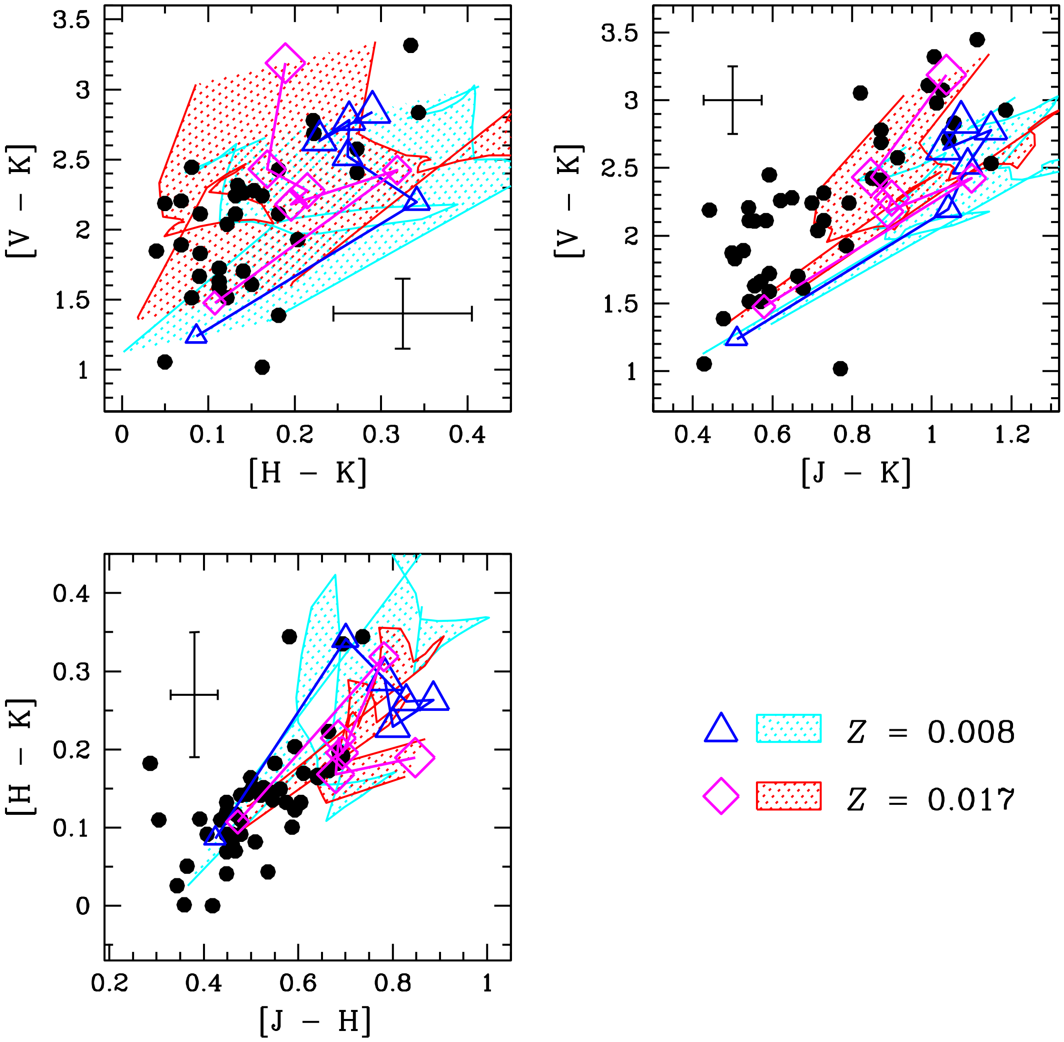

Figure 8. Comparison between models and Magellanic star clusters. *Top left:* $[V-K]$ vs. $[H-K]$; *top right:* $[V-K]$ vs. $[J-K]$; *bottom left:* $[H-K]$ vs. $[J-H]$. Filled circles are clusters compiled from the literature and reddening-corrected by Piovan et al. (2003). Coloured regions represent SSPs with fiducial $\dot{M}$ and expected $\pm 1\sigma$ error bars for $10^5 M_{\odot}$. *Cyan:* $Z = 0.008$ (*cyan*); *red:* $Z = 0.017$. Most of the clusters are younger than 1.5 Gyr; the models range in age between 100 Myr and 1.5 Gyr. Blue triangles and magenta diamonds indicate 0.1, 0.3, 0.5, 0.1, 1.1, and 1.5 Gyr, respectively for $Z = 0.008$ and $Z = 0.017$; increasing symbol size represents increasing age.

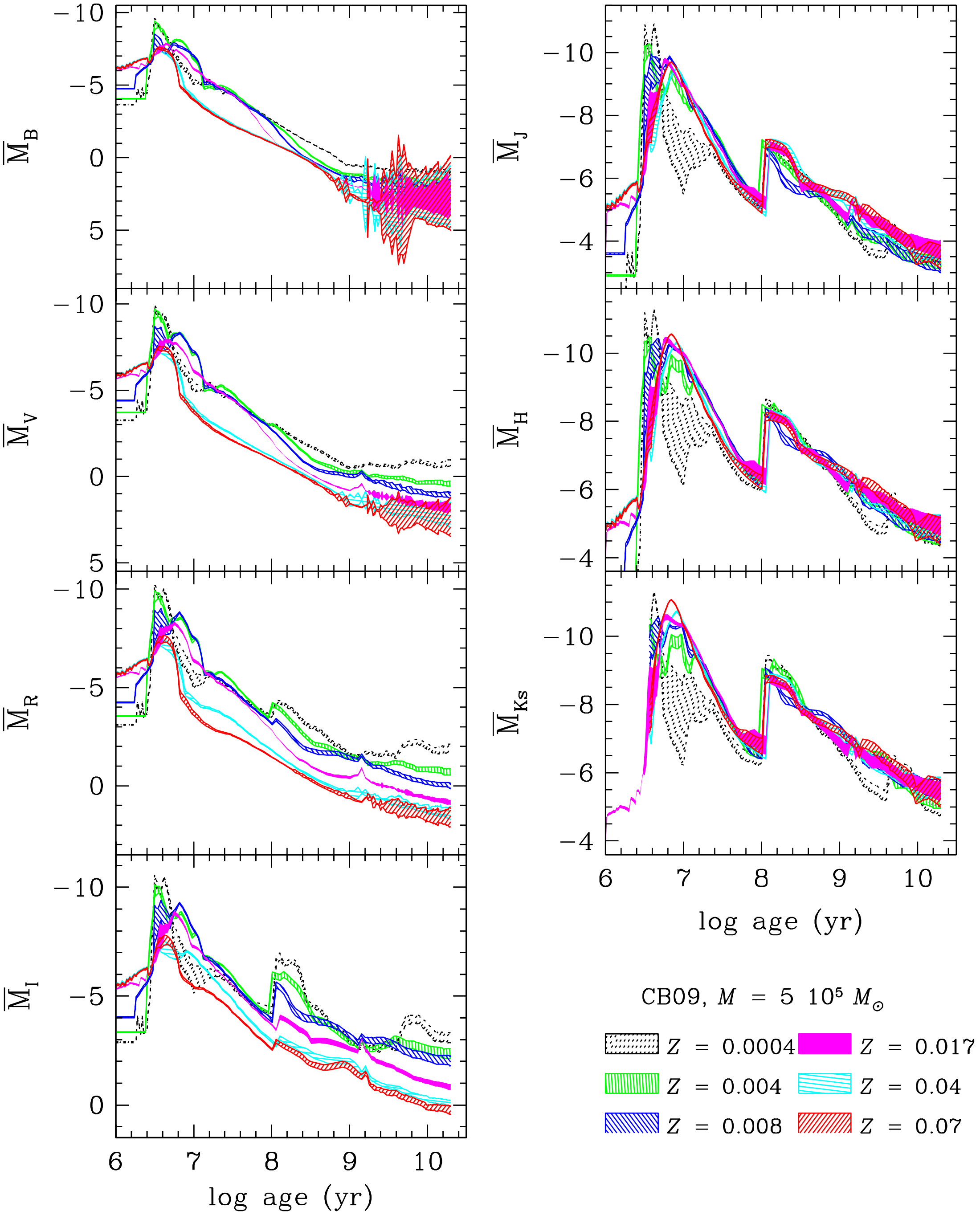

Figure 9. Absolute fluctuation magnitudes vs. log (age) for standard CB09 models with different metallicities. Coloured regions delimit expected ±1σ stochastic errors for stellar populations with 5×10^5 $M_\odot$. *Black-dotted:* $Z = 0.0004$; *green-vertical-hatched:* $Z = 0.004$; *blue-left-hatched:* $Z = 0.008$; *magenta-solid:* $Z = 0.017$; *cyan-horizontal-hatched:* $Z = 0.04$; *red-right-hatched:* $Z = 0.07$.

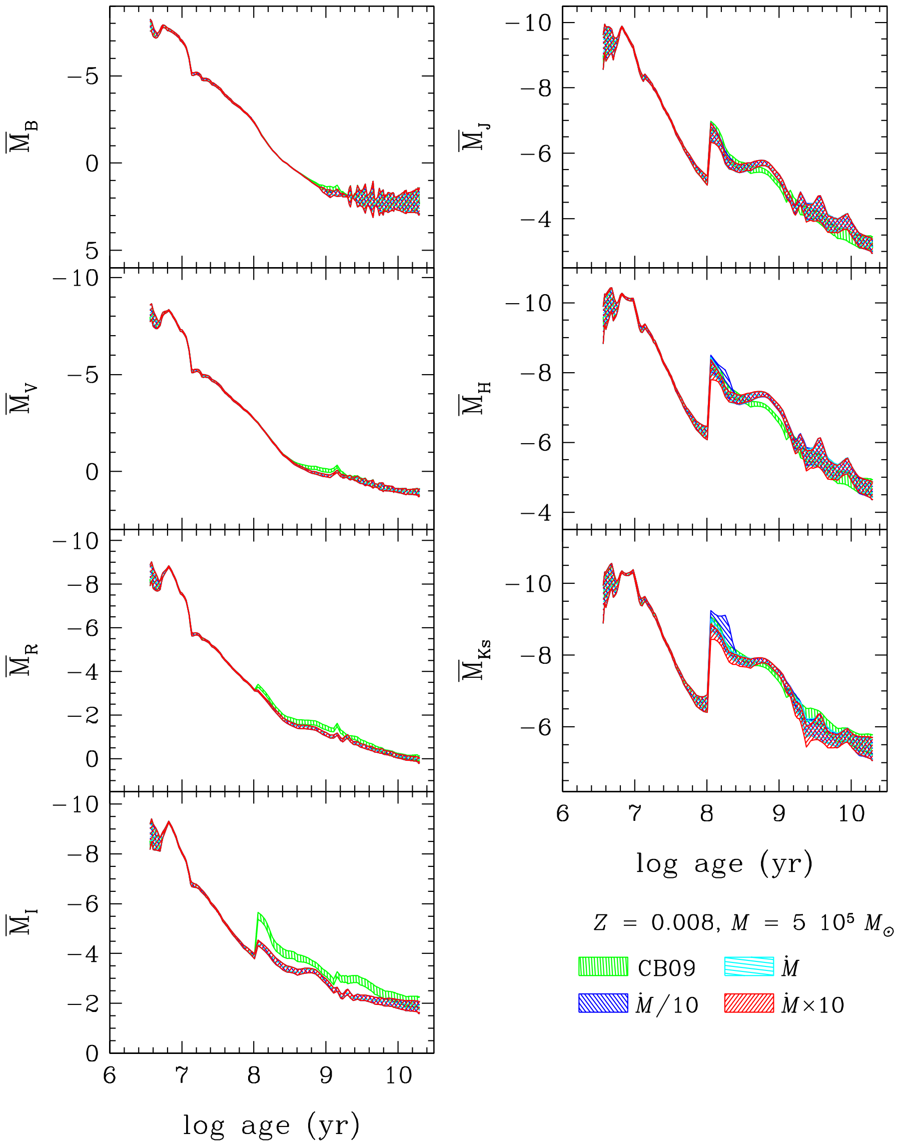

Figure 10. Absolute fluctuation magnitudes vs. log (age) for $Z = 0.008$; models with different mass-loss rates. Coloured regions delimit expected $\pm1\sigma$ stochastic errors for stellar populations with 5×10^5 $M_\odot$. *Green-vertical-hatched:* standard CB09; *blue-left-hatched:* fiducial $\dot{M}/10$; *cyan-horizontal-hatched:* fiducial $\dot{M}$; *red-right-hatched:* fiducial $\dot{M}\times10$.

© 2009 RAS, MNRAS 000, 1–21

Table 5. Characteristic parameters of Magellanic superclusters

Supercluster	Log age (yr)[a]	Z	Mass ($10^6 M_\odot$)[b]	$[V-I]$	$[V-J]$	$[V-H]$	$[V-K_s]$	$[J-Ks]$	$[H-K_s]$	$[J-K_s]$	$\bar{M}_I$	$\bar{M}_J$	$\bar{M}_H$	$\bar{M}_{K_s}$
pre.........	6.78±0.62	0.010±0.005[c]	0.07 ± 0.02	0.34±0.23	0.89±0.26	1.32±0.27	1.64±0.27	0.47±0.18	0.34±0.18	0.81±0.18	-6.10±0.43	-5.86±0.64	-6.76±0.72	-6.78±0.73
I...........	7.51±0.32	0.010±0.005[c]	0.7 ± 0.1	0.62±0.18	1.40±0.21	2.04±0.21	2.28±0.22	0.63±0.14	0.23±0.14	0.86±0.14	-5.79±0.26	-6.77±0.20	-7.60±0.19	-7.77±0.19
II..........	7.88±0.25	0.010±0.005[c]	0.7 ± 0.1	0.54±0.24	1.10±0.24	1.62±0.24	1.78±0.24	0.57±0.13	0.15±0.12	0.72±0.13	-4.76±0.35	-6.59±0.54	-7.34±0.46	-7.58±0.41
III.........	8.21±0.29	0.010±0.005[d]	0.4 ± 0.1	0.49±0.17	1.06±0.18	1.54±0.18	1.68±0.18	0.51±0.11	0.18±0.11	0.51±0.11	-3.03±0.20	-5.97±0.28	-7.11±0.27	-7.46±0.29
IV.........	8.65±0.36	3e-3±2e-3[d]	0.3 ± 0.0	0.51±0.35	1.13±0.33	1.65±0.33	1.86±0.32	0.64±0.16	0.19±0.15	0.83±0.15	-2.37±0.19	-5.43±0.26	-6.67±0.26	-7.12±0.25
V..........	9.09±0.29	4e-3±2e-3[d]	0.5 ± 0.1	1.00±0.23	1.77±0.26	2.38±0.26	2.61±0.26	0.66±0.16	0.26±0.16	0.92±0.16	-2.30±0.11	-4.32±0.16	-5.70±0.19	-6.46±0.23
VI.........	9.45±0.28	2e-3±1e-3[d]	1.8 ± 0.1	1.02±0.28	1.78±0.29	2.39±0.29	2.58±0.29	0.61±0.17	0.17±0.16	0.78±0.17	-1.74±0.18	-3.69±0.20	-5.04±0.23	-5.80±0.29
VII.........	9.82±0.29	7e-4±4e-4[d]	2.8 ± 0.3	1.09±0.33	1.74±0.36	2.26±0.36	2.35±0.35	0.52±0.22	0.08±0.21	0.60±0.22	-2.65±0.35	-2.71±0.26	-3.91±0.36	-4.48±0.51

[a] From the calibration of the S-parameter by Girardi et al. (1995).

[b] Masses from near-IR mass-to-light ratios, CB09 models; errors are equal to the dispersion of the results at J, H, and K_s.

[c] Cohen (1982).

[d] Frogel et al. (1990), assuming $Z_\odot = 0.017$.

Given the significantly greater depth of their *HST* data, Raimondo et al. were able to measure both the numerator and denominator of equation 1 using resolved stars. They determined absolute V and I fluctuation magnitudes with the same LMC distance modulus $(m-M)_0 = 18.5$. The comparison of the described cluster data with the results of the models presented in this work is shown in Figures 11 to 14.

Figures 11 and 12[14] present V, I, J, H, and K_s SBF absolute magnitudes vs. log (age) of young and intermediate-age MC clusters. Optical ($\bar{M}_V$ and $\bar{M}_I$) measurements of individual, rich clusters have been taken from Raimondo et al. (2005). These data are shown as solid circles. For this work, we have recalculated near-IR fluctuation values for the superclusters as described above, and calculated $\bar{M}_I$, as well. These data are shown as empty triangles. As seen before, SBF measurements are not capable of discriminating between different mass-loss rates.

In the near-IR, there is a good overall match between models and data. In the optical V and I-bands, there is a tendency for the data of single MC clusters first published by Raimondo et al. (2005) to fall below the model values. Among these clusters, the problem is most acute for NGC 1805 ($\log t = 7.00 \pm 0.20$), NGC 1818 ($\log t = 7.40 \pm 0.30$), and Hodge 14 ($\log t = 9.30 \pm 0.10$). In the case of Hodge 14, severe field contamination forced Raimondo et al. to analyse only a small area (i.e., mass) of the cluster; the resulting larger stochastic uncertainty is reflected by the SBF magnitudes error bars. For NGC 1805 and NGC 1818, they mention a possible 10% incompleteness of the brightest 3 mag of cluster stars within $7\overset{''}{.}2$ from the centre, that in principle is accounted for by the shown error bars. A logical conclusion –also reached by Raimondo et al. (2005)– is that the number of stars in these individual globular clusters is not enough to adequately sample the brightest, rarest, TP-AGB stars. Additional systematic effects that might impact the data of both NGC 1805 and the pre-SWB supercluster of González et al. have been already discussed in section 5.2.

Results for clusters with $Z \sim 0.002$ are shown in Fig. 13. Figure 14 compares SBF measurements of old MC clusters, with $Z \sim 0.0007$, to models with $Z = 0.001$. The agreement between models and data is roughly the same if models with $Z = 0.0004$ are used instead. For the one "supercluster" shown and contrariwise to what we had seen so far, we find that the fit between models and data in the optical is better than the match in the near-IR. Since Raimondo et al. (2005) do not use our same mapping between SWB type and age (and thus metallicity), we show their four oldest clusters in both figures 13 and 14. Their quoted SWB type is VI, like our one supercluster displayed in Fig. 13 as an empty triangle, whereas their listed ages are all over 10 Gyr old, i.e., older than our type VII supercluster, and hence we plot them too in Fig. 14.

6 MID-INFRARED SBF MEASUREMENTS AND FUTURE WORK.

So, can SBF measurements at all, with their sensitivity to the brightest stars of a population, provide some insight about the mass-loss parameters of unresolved stellar populations? Figure 15 shows absolute fluctuation magnitudes vs. log (age), again for $Z = 0.008$, but this time in the mid-IR bands observed by the Spitzer Space Telescope. According to this figure, in the mid-IR one could begin to distinguish intermediate age stellar populations with different mass-loss rates, to the point that it might be worthwhile to start exploring the effects of other dust mixtures and even of the dust chemistry in the stellar envelopes on the integrated properties of stellar populations. In a forthcoming paper, we will compare models in the mid-IR with Spitzer observations of stars in the Large Magellanic Cloud.

7 SUMMARY AND CONCLUSIONS.

We have presented optical and IR broad-band colours and SBF magnitudes computed from single stellar population synthesis models, where the mass-loss rates in the CB09 evolutionary tracks have been used to produce spectra of TP-AGB stars, taking into account the radiative transfer in their dusty circumstellar envelopes. Star plus envelope SEDs have been processed also for $\dot{M}$ one order of magnitude above and below the fiducial mass-loss rates; for mass-loss rates different from the original ones in the tracks, stellar configurations and lifetimes have been adjusted. Next, we have compared our models to optical and near-IR data of single AGB stars and Magellanic star clusters.

Even though mass-loss regulates lifetimes, luminosities, and effective temperatures of stars in the AGB phase, and hence their numbers and colours, it turns out that broad-band optical and near-IR colours and SBF measurements of stellar populations cannot discern global variations in mass-loss rate. Worse even than for single stars, the selection effects that preclude detection of single stars away from the "cliff" in a core mass vs. luminosity plot (stars either losing mass too slowly for the mass-loss to be observed or too fast for the star to be detected, due both to lifetime and obscuration) make differences in mass-loss rate across whole populations completely unnoticeable.[15]

We predict that SBF measurements in the mid-IR could begin to pick out intermediate age stellar populations where the stars lose mass with rates away from the cliff line, and help determine if such deviations actually correlate with metallicity.

ACKNOWLEDGMENTS

It is our pleasure to thank three anonymous referees for their very thorough and helpful reports. R.A.G.-L. recognizes the

---

[14] Note that the x-axes in figures 12, 13, and 14 start only at log (age) = 7.4, in order to highlight the features of the models at older ages.

[15] According to a very recent article (Raimondo 2009) that appeared while the present work was being refereed, an extinction A_V between 0.01 and 1 mag is adequate to fit near-IR data of AGB stars. Raimondo concludes that dust-enshrouded AGB stars, with higher opacities, would rather leave their imprint at longer wavelengths.

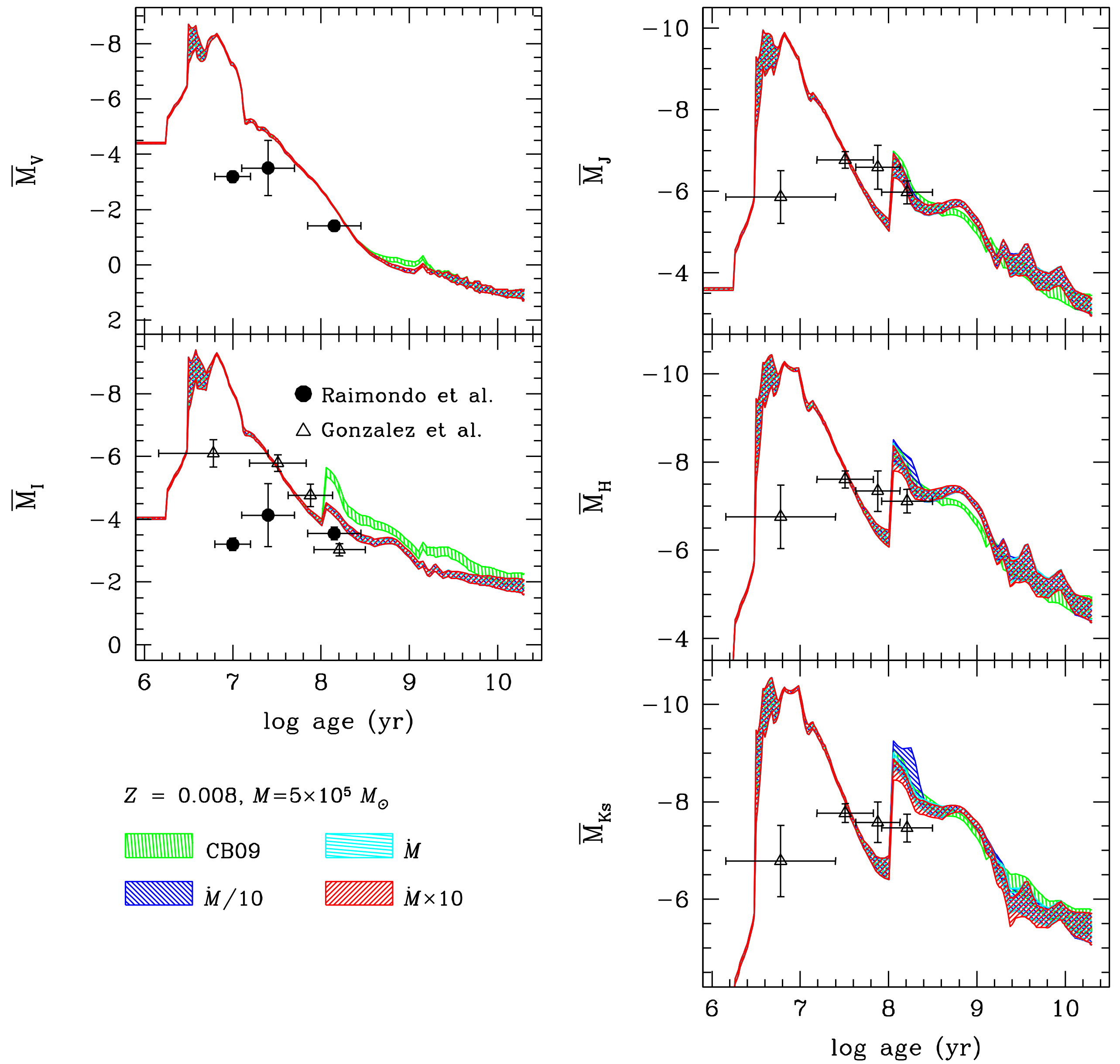

Figure 11. SBFs of Magellanic star clusters I. Observations of young and intermediate-age MC star clusters are compared to models with $Z = 0.008$. $\pm1\sigma$ stochastic uncertainties are shown for stellar populations with 5 $\times10^5$ $M_\odot$, coded as in Figure 10. *Solid circles* are $\bar{M}_V$ and $\bar{M}_I$ measurements for globular clusters from Raimondo et al. (2005); *empty triangles* are $\bar{M}_I$ and near-IR SBF measurements for artificial MC "superclusters" (see González et al. 2004, 2005).

support of CONACyT, México, and DGAPA, UNAM. She also thanks M. Matsuura, J. Blakeslee, P. D'Alessio, J. van Loon, K.-P. Schröder, S. Kurtz, L. Piovan, and M. Cerviño. Sundar Srinivasan and Margaret Meixner made their catalog of AGB candidates in the Magellanic Clouds available to us in advance of publication.

We thank the whole DENIS Team, and especially its PI, N. Epchtein, for making available de DENIS data. The DENIS project is supported, in France by the Institut National des Sciences de l'Univers, the Education Ministry and the Centre National de la Recherche Scientifique, in Germany by the State of Baden Würtemberg, in Spain by the DGICYT, in Italy by the Consiglio Nazionale delle Ricerche, in Austria by the Fonds zur Förderung der wissenschaftlichen Forschung and the Bundesministerium für Wissenschaft und Forschung.

This research has made use of the VizieR Service and the SIMBAD database at the Centre de Données Astronomiques de Strasbourg, as well as NASA's Astrophysics Data System Abstract Service.

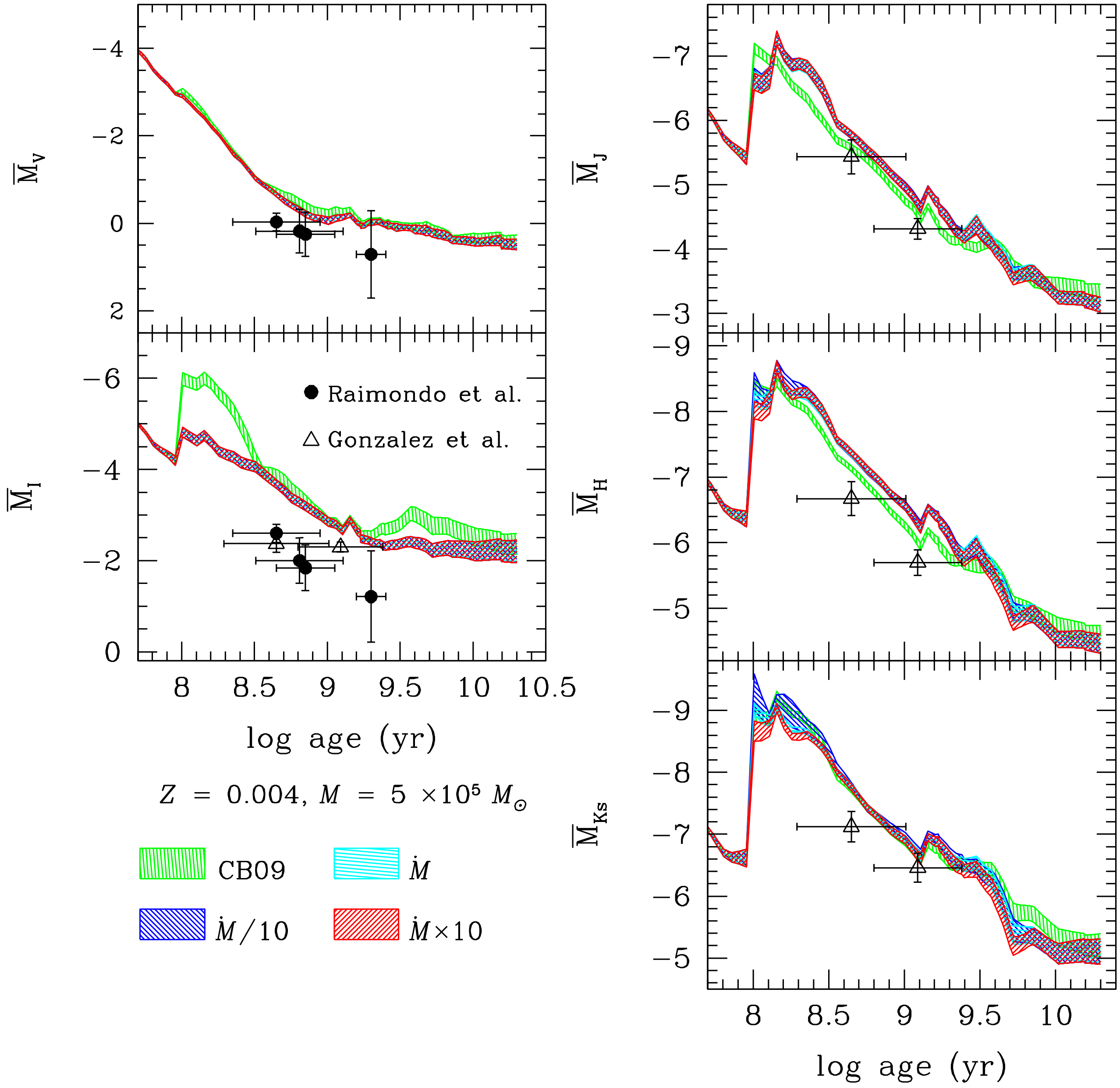

Figure 12. SBFs of Magellanic star clusters II. Observations of intermediate-age MC clusters are compared to models with $Z = 0.004$. $\pm 1\sigma$ stochastic uncertainties are shown for stellar populations with 5×10^5 $M_\odot$, coded as in Figure 10.

APPENDIX A: MODELLING THE STELLAR PLUS ENVELOPE EMISSION.

A1 Mass-loss rate and stellar parameters.

We treat $\dot{M}$ as the independent parameter, and modify L, using Figure 2 in Bowen & Willson (1991) (reproduced as Figure 14 in Marigo & Girardi 2007). The former gives lines of constant $\dot{M}/M$ in the log M vs. log L plane, for dusty Miras with solar metallicity.

Next, we find the modified stellar radius from the Iben (1984) radius-luminosity-mass relation for evolving AGB stars, reproduced as equation 3 in Bowen & Willson (1991),[16] and calculate the effective temperature using $L = R^2(T_{\rm eff}/5770)^4$.

This is the inverse of the procedure used by Marigo & Girardi (2007) to determine $\dot{M}$ for an oxygen-rich

---

[16] $R = 312(L/10^4)^{0.68}(M/1.175)^{-0.31S}(Z/0.001)^{0.088(l/H_p)^{-0.52}}$, where L and M are in solar units, (l/H_p) is the ratio of mixing length to pressure scale height, and $S = 0$ for $M \leqslant 1.175$ and $S = 1$ otherwise.

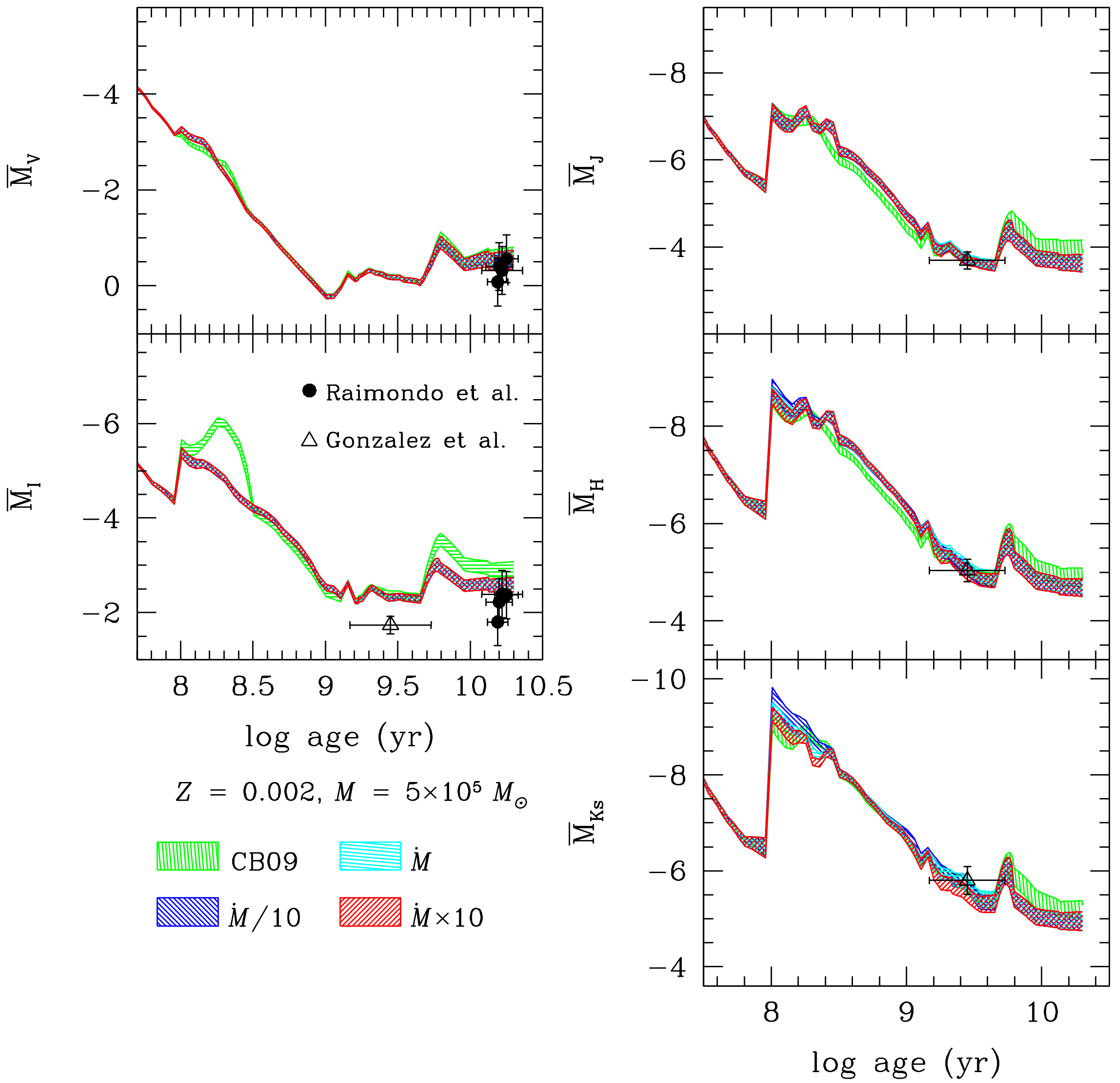

Figure 13. SBFs of Magellanic star clusters III. Observations of old MC clusters are compared to models with $Z = 0.002$. $\pm1\sigma$ stochastic uncertainties are shown for stellar populations with $5 \times 10^5\ M_\odot$, coded as in Figure 10. According to their reported SWB type (VI), Raimondo's four oldest MC clusters belong here.

AGB star (from mass and Z they calculate period, next radius, then luminosity, and ultimately mass-loss rate).

Once the new L, R, and T_eff are known, and assuming the energy available to a star of type i during an evolutionary phase is constant (i.e., the fuel consumption theorem, Renzini & Buzzoni 1986), the length t_2 of the extrapolated mass-loss phase can be derived from the relation $L_1t_1 = L_2t_2$, where subscript 1 denotes original parameters and subscript 2 represents the extrapolated ones. If, furthermore, we assume that the weight w_i of a stellar type i (i.e., the number of stars of initial mass m going through an evolutionary phase ph, per unit mass of the population) is proportional to the time spent by such stars in the phase, then $w_{i,2}/w_{i,1} = t2/t1 = L1/L2$. $w_{i,1} \equiv 1$, by definition, and $w_{i,2}$ is the same for all stars with the same metallicity, once the extrapolation factor is fixed, with the following exceptions. There are occasions when the product of the mass-loss rate and the phase length derived with the above procedure is greater than the stellar core mass at the beginning of the stage, M_evst. In these cases, $w_{i,2} = M_\mathrm{evst}/\dot{M}/t_2$, and the weight of the subsequent stage will be zero (i.e., the star will not reach the following stage). In other instances, the dust-

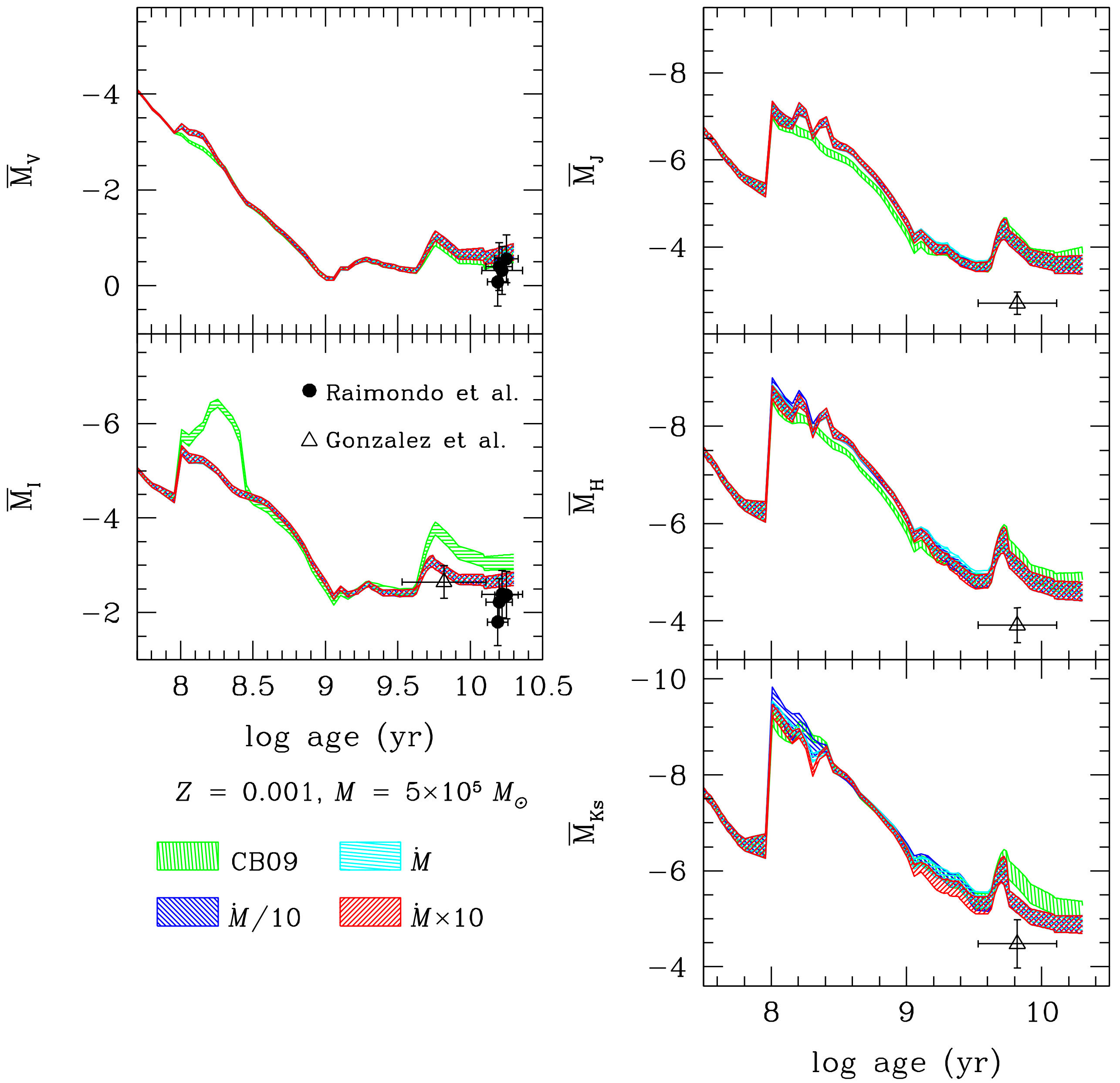

Figure 14. SBFs of Magellanic star clusters IV. Observations of old MC star clusters are compared to models with $Z = 0.001$. $\pm 1\sigma$ stochastic uncertainties are shown for stellar populations with 5×10^5 $M_\odot$, coded as in Figure 10. According to their reported ages, Raimondo's four oldest MC clusters belong in this figure.

to-mass ratio Ψ diverges (see eq. A17 in Section A2.2 below), consequently the shell opacity also diverges (see eq. A3, Section A2), and hence we assign $w_{i,2} = 0$ to such stars in view of their very heavy obscuration. In general, the mass lost in any given stage with modified mass-loss rate will be different from the mass lost in the original track, so an adjustment to the parameters of the subsequent stage will be needed. Logically, we first rectify the stellar mass $M_{\rm evst}$ and next the luminosity L_1, moving along a line of constant $\dot{M}/M$ in the aforementioned Figure 2 of Bowen & Willson (1991). From then on, we repeat the procedure outlined here: we first modify $\dot{M}$, and then derive L_2, R_2, $T_{eff,2}$, t_2, $w_{i,2}$.

Fundamental mode (FM) pulsation periods P_0 also change with the stellar configuration. To adjust these, we use eq. 12 in Marigo & Girardi (2007):

$$\begin{aligned}\log\,(P_0/\mathrm{days}) = &-2.07\ +\ 1.94\,\log\,(R/R_\odot)\\ &-0.9\,\log\,(M/M_\odot)\ (\mathrm{if}\ M\ <\ 1.5M_\odot)\\ = &-2.59\ +\ 2.2\,\log\,(R/R_\odot)\end{aligned}$$

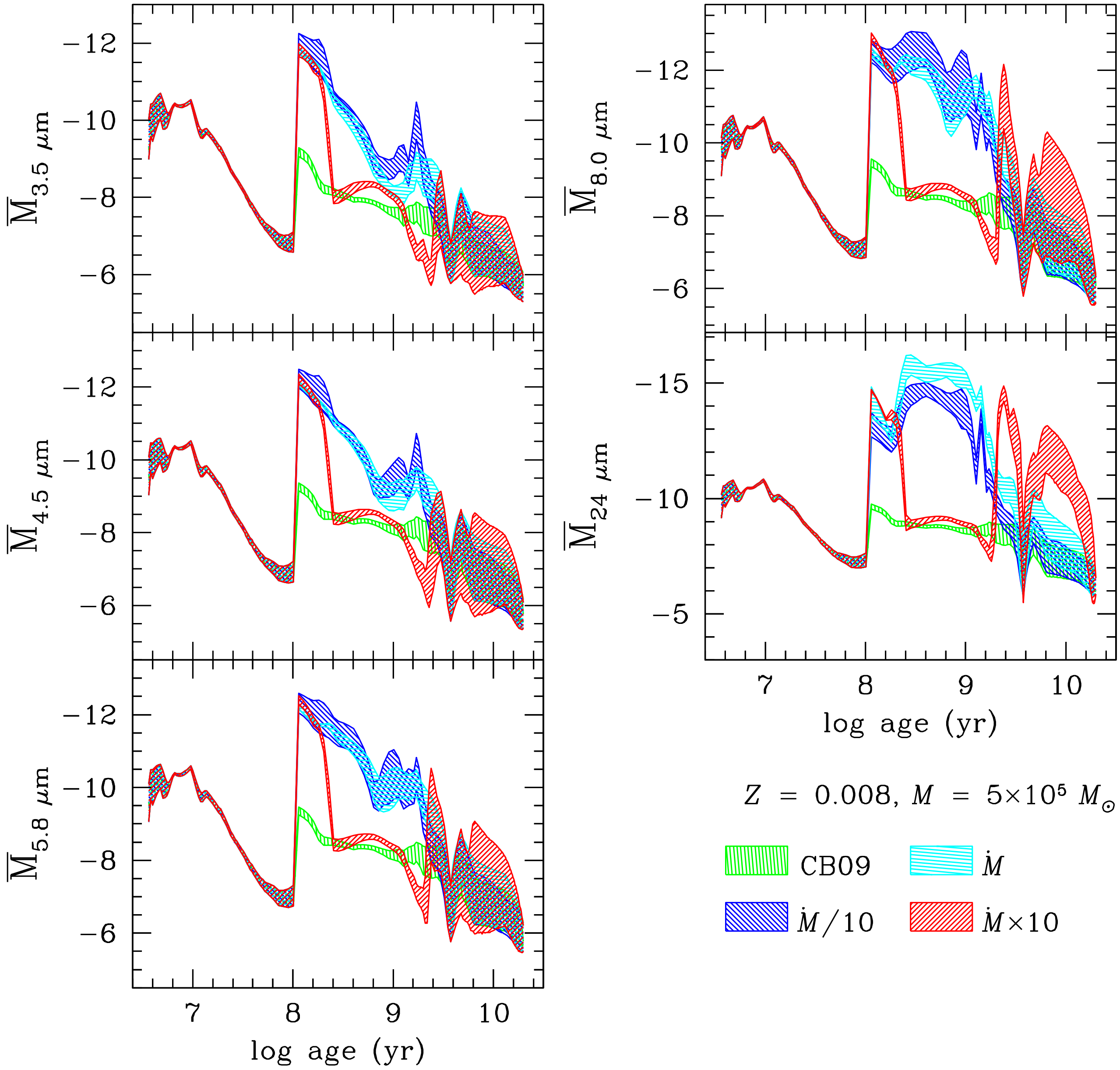

Figure 15. Mid-IR absolute fluctuation magnitudes vs. log (age) for $Z = 0.008$; models with different mass-loss rates. Coloured regions, coded as in Figure 10, delimit expected $\pm 1\sigma$ stochastic errors for stellar populations with $5 \times 10^5\ M_\odot$.

$$- \ 0.83 \ \log\,(M/M_\odot) \ - \ 0.08 \ \log\,(Z/10^{-3}) \\ + \ 0.25(Y - 0.3) \ (\text{if } M \ > \ 2.5M_\odot). \qquad \text{(A1)}$$

Z and Y are, respectively, metallicity and helium content by mass; for M between 1.5 and 2.5 $M_\odot$, log P_0 is interpolated linearly, with log M as the independent variable. In the case of C-rich stars in the superwind phase, another parameter that changes with $\dot{M}$ is the C/O ratio. For this, we use eq. 23 in Marigo & Girardi (2007):[17]

$$\log\,[\dot{M}/(M_\odot \text{yr}^{-1})] = - \ 4.529 \\ - \ 6.849 \ \log\,(T_{\rm eff}/2600\ \text{K}) \ + \ 1.527 \ \log\,(L/10^4 L_\odot) \\ - \ 1.997 \ \log\,(M/M_\odot) \ + \ 0.995 \ \log\,(P_0/650 \ \text{days})$$

---

[17] This expression is similar to that proposed by Wachter et al. (2002) for winds driven by radiation pressure on dust grains, except that it contains an explicit dependence on the C/O ratio. Eq. 23 of Marigo & Girardi (2007) has an error: the minus sign in front of log P_0 should be a plus, as it appears here and in Wachter et al. (2002).

$$+\ 0.672\ \log\left(\frac{C/O}{1.5}\right). \qquad \text{(A2)}$$

Eq. A2 is valid for $\dot{M} \geqslant 10^{-6}\ M_\odot\ \mathrm{yr}^{-1}$.

A2 Parameters of the dusty envelopes.

The effect of dust on the stellar SEDs has to be included, both for stars in the original tracks and for those whose mass-loss rates and stellar parameters have been modified. To this end, we follow the procedure outlined by Piovan et al. (2003) and Marigo et al. (2008) based on, respectively, Ivezić & Elitzur (1997) and Elitzur & Ivezić (2001). One very important input parameter to produce the SED through radiative transfer calculations is the optical depth, τ, of the envelope.

For a star of luminosity L and effective temperature T_{eff}, losing mass at a rate $\dot{M}$, with dust expansion velocity v_{exp} and dust-to-gas ratio Ψ, the optical depth at wavelength λ is approximately (see eq. 12 of Piovan et al. 2003):

$$\tau_\lambda \simeq \frac{\Psi \dot{M} \kappa_\lambda}{4\pi v_{\mathrm{exp}}} \frac{1}{r_{\mathrm{in}}}, \qquad \text{(A3)}$$

where κ_λ is the extinction coefficient per unit mass and r_{in} is the dusty shell internal radius.

If the shell is optically thick to radiation of wavelength λ, we can write

$$L = 4\pi R^2 \sigma T_{\mathrm{eff}}^4 = 4\pi r_{\mathrm{in}}^2 \sigma T_{\mathrm{d}}^4, \qquad \text{(A4)}$$

and

$$r_{\mathrm{in}} = \left(\frac{L_\odot}{4\pi\sigma T_{\mathrm{d}}^4}\right)^{1/2} \left(\frac{L}{L_\odot}\right)^{1/2}, \qquad \text{(A5)}$$

where R is the stellar radius, σ is the Stefan-Boltzmann constant, and T_{d} is the dust condensation temperature at r_{in}. Adopting $T_{\mathrm{d}} = 1000$ K when C/O < 0.97 and $T_{\mathrm{d}} = 1500$ K when C/O $\geqslant 0.97$,

$$r_{\mathrm{in}} = 2.37 \times 10^{12} \left(\frac{L}{L_\odot}\right)^{1/2} \mathrm{cm\ (for\ O-rich\ stars)}$$

$$r_{\mathrm{in}} = 1.05 \times 10^{12} \left(\frac{L}{L_\odot}\right)^{1/2} \mathrm{cm\ (for\ carbon\ stars)}; \qquad \text{(A6)}$$

in any case (see eq. 4 of Marigo et al. 2008):

$$\tau \propto \dot{M} \Psi v_{\mathrm{exp}}^{-1} L^{-0.5}. \qquad \text{(A7)}$$

A2.1 Wind expansion velocity.

Based on the solution to the dust-wind problem by Elitzur & Ivezić (2001), Marigo et al. (2008) express the wind expansion velocity v_{exp} as a function of $\dot{M}$, L, Ψ, and other dust parameters as follows:

$$v_{\mathrm{exp}} = \left(A\dot{M}_{-6}\right)^{1/3} \left(1 + B\frac{\dot{M}_{-6}^{4/3}}{L_4}\right)^{-1/2} \mathrm{km\ s^{-1}}, \qquad \text{(A8)}$$

where $\dot{M}_{-6}$ is the mass-loss rate in units of $10^{-6} M_\odot\ \mathrm{yr}^{-1}$ and L_4 is the stellar luminosity in units of $10^4 L_\odot$.

The parameters A and B are defined as:

$$A = 3.08 \times 10^5\ T_{\mathrm{d3}}^4\ Q_\star \sigma_{22}^2\ \chi_0^{-1} \qquad \text{(A9)}$$

$$B = \left[2.28 \frac{Q_\star^{1/2} \chi_0^{1/4}}{Q_V^{3/4} \sigma_{22}^{1/2} T_{\mathrm{d3}}}\right]^{-4/3}. \qquad \text{(A10)}$$

T_{d3} is the dust condensation temperature in units of 10^3 K; $Q_\star$ is the Planck average[18] of the efficiency coefficient for radiation pressure, evaluated at T_{eff}, and Q_V is the efficiency coefficient for absorption at the visual range. χ_0 is defined as:

$$\chi_0 = \frac{Q_P(T_{\mathrm{eff}})}{Q_P(T_{\mathrm{d}})}, \qquad \text{(A12)}$$

with $Q_P(T)$ the Planck average of the absorption efficiency at temperature T, whereas σ_{22} is σ_{gas}, the dust cross-section per gas particle, in units of 10^{-22} cm^2, and

$$\sigma_{\mathrm{gas}} = \pi \left(\frac{a}{2}\right)^2 \frac{n_{\mathrm{dust}}}{n_{\mathrm{gas}}}\ \mathrm{cm}^2, \qquad \text{(A13)}$$

with a the mean size of the dust grains in cm (assumed to be the same for all grains), and n_{dust} and n_{gas} the number densities in cm^{-3} of, respectively, the dust and gas particles.

σ_{gas} can be written as a function of Ψ, the dust-to-gas ratio, as follows:

$$\Psi = \frac{\rho_{\mathrm{dust}}}{\rho_{\mathrm{gas}}} = \frac{\frac{4}{3}\pi\left(\frac{a}{2}\right)^3 \rho_{\mathrm{grain}} n_{\mathrm{dust}}}{A_{\mathrm{gas}} m_H n_{\mathrm{gas}}}, \qquad \text{(A14)}$$

where ρ_{dust} and ρ_{gas} are the density of matter in the form of dust and gas, respectively, in g cm^{-3}. $A_{\mathrm{gas}} \simeq 4/(4X_{\mathrm{H}} + X_{\mathrm{He}})$ is the mean molecular weight of the gas in units of the H atom mass, $m_{\mathrm{H}} = 1.674 \times 10^{-24}$ g, assuming that all the gas is composed by H and He, with respective mass fraction abundances X_{H} and X_{He}. Substituting eq. A14 into eq. A13,

$$\sigma_{\mathrm{gas}} = \frac{3}{2} \frac{A_{\mathrm{gas}} m_{\mathrm{H}}}{a\ \rho_{\mathrm{grain}}} \Psi. \qquad \text{(A15)}$$

The values of Q_V for silicates, silicon carbide, and amorphous carbon (see below, Subsection A2.2 and Section A3) are taken from Table 3 in Marigo et al. (2008); the values of $Q_\star(T_{\mathrm{eff}})$, $Q_P(T_{\mathrm{eff}})$, and $Q_P(T_{\mathrm{d}})$ (each one for all the same materials) are interpolated from the quantities tabulated there, taking temperature as the independent variable.[19]

Clearly, eq. A8 is valid as long as there is enough dust condensation to drive an outflow. This condition sets the minimum mass-loss rate (Elitzur & Ivezić 2001):

$$\dot{M}_{\mathrm{min}} = 3 \times 10^9 \frac{M^2}{Q_\star \sigma_{22}^2 L_4 T_{k3}^{1/2}}\ M_\odot\ \mathrm{yr}^{-1}. \qquad \text{(A16)}$$

---

[18] The Planck mean of a function $Q(\lambda)$ is given by (Blanco et al. 1983):

$$< Q(T) >= \frac{\int\limits_0^\infty B(\lambda,T) Q(\lambda) \mathrm{d}\lambda}{\int\limits_0^\infty B(\lambda,T) \mathrm{d}\lambda}, \qquad \text{(A11)}$$

where $B(\lambda, T)$ is the Planck function at a temperature T.

[19] As seen in Section A2, $T_{\mathrm{d}} = 1000$ K for C/O < 0.97, and $T_{\mathrm{d}} = 1500$ K for C/O $\geqslant 0.97$.

T_{k3} is the kinetic temperature (in units of 10^3 K) at the inner boundary of the dust shell, which is assumed to be equal to the dust condensation temperature, T_{d3}. At smaller values of $\dot{M}$, dust cannot drive a wind but may still form in the circumstellar envelope. Following Marigo et al. (2008), we handle this situation by setting $v_{\mathrm{vexp}} = v_{\mathrm{exp}}(\dot{M}_{\mathrm{min}})$, while using the actual $\dot{M}$ to calculate the opacity of the envelope.

A2.2 Dust-to-gas ratio.

If dust and gas share the same outflow velocity, the dust-to-gas ratio can also be written as the quotient between mass-loss in the form of dust and mass-loss in the form of gas:

$$\Psi = \frac{\dot{M}_{\mathrm{dust}}}{\dot{M}_{\mathrm{gas}}} = \frac{\dot{M}_{\mathrm{dust}}}{\dot{M} - \dot{M}_{\mathrm{dust}}}. \tag{A17}$$

We calculate $\dot{M}_{\mathrm{dust}}$ as described by Marigo et al. (2008), who follow the formalism by Ferrarotti (2003); Ferrarotti & Gail (2006). Summarizing,

$$\dot{M}_{\mathrm{dust}} = \sum_i \dot{M}_{\mathrm{dust},i}, \tag{A18}$$

with the summation over several dust species, written as

$$\dot{M}_{\mathrm{dust},i} = \dot{M} X_{\mathrm{seed}} \left(\frac{A_{\mathrm{dust},i}}{A_{\mathrm{seed}}} \right) f_{\mathrm{dust},i}. \tag{A19}$$

Here, $A_{\mathrm{dust},i}$ is the mean molecular weight of the dust species, X_{seed} is the total mass fraction of the seed element in the circumstellar shell, and A_{seed} is its atomic weight. The seed element is the least abundant one among those needed to form the considered dust species, and hence limits its supply. Finally, $f_{\mathrm{dust},i}$ is the fraction of the seed element condensed into dust grains, that for each dust species is calculated as a function of $\dot{M}$ and C/O ratio using the analytic fits in Ferrarotti (2003), as shown below.

Stars with C/O < 0.97. In these conditions, there are enough oxygen atoms to form silicate-type dust, and:

$$\frac{dM_{\mathrm{dust}}}{dt} = \frac{dM_{\mathrm{sil}}}{dt} = \dot{M} X_{\mathrm{Si}} \frac{A_{\mathrm{sil}}}{A_{\mathrm{Si}}} f_{\mathrm{sil}}, \tag{A20}$$

where A_{Si} is the atomic weight of silicon, A_{sil} is the effective molecular weight of the silicate dust, and f_{sil} is the condensation degree, also of the silicate dust. Given the dust mixture we use here for O-rich stars (see below, Section A3), the condensation degree includes the contributions from amorphous and crystalline silicates:

$$f_{\mathrm{sil}} = f_{\mathrm{warm}} + f_{\mathrm{cold}} + f_{\mathrm{ens}} + f_{\mathrm{fors}}, \tag{A21}$$

where subscripts stand for warm silicate, cold silicate, enstatite, and forsterite dust. On the other hand, the effective molecular weight of the silicate dust mixture is:

$$A_{\mathrm{sil}} = (f_{\mathrm{warm}} A_{\mathrm{warm}} + f_{\mathrm{cold}} A_{\mathrm{cold}} + f_{\mathrm{ens}} A_{\mathrm{ens}} + f_{\mathrm{fors}} A_{\mathrm{fors}}) / f_{\mathrm{sil}}. \tag{A22}$$

The degree of condensation of silicate type dust is found from the analytic fit in Ferrarotti (2003), used also by Marigo et al. (2008):

$$f_{\mathrm{sil}} = 0.8 \frac{\dot{M}_{-6}}{\dot{M}_{-6} + 5} \sqrt{\frac{Y_{\mathrm{C},1} - Y_{\mathrm{C}}}{Y_{\mathrm{C},1}}}. \tag{A23}$$

Here, $Y = X/A$ is abundance in molecules g^{-1}, and $Y_{\mathrm{C},1} = Y_{\mathrm{O}} - 2Y_{\mathrm{Si}}$ (Ferrarotti & Gail 2006). Once f_{sil} is determined for each star, the relative degrees of condensation of crystalline and amorphous silicates are set according to the optical depth of the envelope, as described below (Section A3).[20]

Stars with C/O ⩾ 0.97. These are C-rich stars, since the dust mixture in their envelopes is dominated by carbon. As stated below in Section A3, we consider two dust constituents, SiC and amorphous carbon (AMC), such that:

$$\frac{dM_{\mathrm{dust}}}{dt} = \frac{dM_{\mathrm{SiC}}}{dt} + \frac{dM_{\mathrm{AMC}}}{dt}, \tag{A24}$$

where the first addend corresponds to the silicon carbide dust and the second, to the amorphous carbon dust. Furthermore,

$$\frac{dM_{\mathrm{AMC}}}{dt} = \dot{M} X_{\mathrm{C}} f_{\mathrm{AMC}}. \tag{A25}$$

X_{C} is the carbon abundances by mass; we take the current atmospheric value, solar scaled, or $X_{\mathrm{C}} = (\mathrm{C/O}) X_{\mathrm{O},\odot} (Z/Z_{\odot})$, where $X_{\mathrm{O},\odot}$ is the solar mass fraction abundance of oxygen taken from Grevesse & Sauval (1998).[21]

Finally, the degree of condensation of carbon is found from Ferrarotti (2003):[22]

$$f_{\mathrm{AMC}} = 0.5 \frac{\dot{M}_{-6}}{\dot{M}_{-6} + 5} \left(\frac{\mathrm{C}}{\mathrm{O}} - 0.97 \right). \tag{A26}$$

Once f_{AMC} is found, the relative degree of condensation of SiC dust is set according to the opacity of the envelope, as described below (Section A3).

A2.3 Extinction coefficient.

In order to determine κ_λ, we follow the procedure by Piovan et al. (2003). The mass extinction coefficient can be written as:

$$\kappa_\lambda = \frac{\sum_i n_{\mathrm{dust},i} \sigma_{\mathrm{dust},i}}{\rho_{\mathrm{dust}}}, \tag{A27}$$

with the summation over all types of grains in the dust mixture, and where the ith type of grain has number density $n_{\mathrm{dust},i}$ cm^{-3}, and cross-section for radiation-dust interactions $\sigma_{\mathrm{dust},i}$ cm^2; ρ_{dust} (g cm^3) is, again, the density of matter in the form of dust, and $\sigma_{\mathrm{dust},i}(a) = \pi a^2 Q_{\mathrm{ext}}(i)$, where $Q_{\mathrm{ext}}(i)$ are the extinction coefficients. If $m_{\mathrm{dust},i}$ is the mass of the ith type of dust grains, and we introduce the mass abundance $\chi_i = n_{\mathrm{dust},i} m_{\mathrm{dust},i} / \rho_{\mathrm{dust}}$:

$$\kappa_\lambda = \sum_i \chi_i \frac{\sigma_{\mathrm{dust},i}}{m_{\mathrm{dust},i}}. \tag{A28}$$

---

[20] For the cold and warm amorphous silicates we use the following formulae, respectively (Dorschner et al. 1995): $\mathrm{Mg_{0.8}Fe_{1.2}SiO_4}$; $\mathrm{Mg_{0.4}Fe_{0.6}SiO_3}$.

[21] For consistency with Marigo & Girardi (2007), and with the different works by Ferrarotti and collaborators.

[22] Ferrarotti writes (C/O - 1), but we change it to (C/O - 0.97), to avoid the possibility of negative degrees of condensation.

Going back to eq. A3, one can see that dust optical depth is a function of κ_λ, but then κ_λ is a function of the optical depth, because the dust composition is itself a function of τ_λ. Consequently, an iterative procedure is needed to determine the dust optical depth.

A3 Implementation of the envelopes with DUSTY.

The DUSTY code includes the dependence of the wind speed on stellar luminosity and metallicity (through the gas-to-dust ratio of the envelope), and the drift speed between the dust and the gas. The code outputs spectral *shapes*, that can then be scaled to energy flux by multiplying by the stellar luminosity, and dividing by $4\pi d^2$. DUSTY offers a broad choice of input parameters, specifically in regard to the dust chemical composition and grain size distribution.

We adopt here the dust mixtures introduced by Suh (1999, 2000, 2002), with the aim of fitting observations of individual stellar spectra, and later used by Piovan et al. (2003) in SSP models. Suh has calculated optical constants for siliceous and carbonaceous compounds that are consistent with the Kramers-Kronig dispersion relations and, at the same time, yield models of dusty envelopes that fit observed properties of AGB stars. For O-rich stars, Suh (2002) proposes combinations of both amorphous and crystalline silicate grains (enstatite, $MgSiO_3$, and forsterite, Mg_2SiO_4), in proportions that depend on the optical depth of the dusty shell: (*a*) for stars with the lowest mass-loss rates and thin shells, where the 10 μm silicate feature is observed in emission ($\tau_{10} \leqslant 3$), a blend of 90% warm amorphous silicate, 5% enstatite, and 5% forsterite grains; (*b*) for stars with low mass-loss rates and moderately optically thick shells ($3 < \tau_{10} \leqslant 15$), 90% cold amorphous silicate, 5% enstatite, and 5% forsterite grains; (*c*) for stars with high mass-loss rates and optically thick shells ($\tau_{10} > 15$), 80% cold amorphous silicate, 10% enstatite, and 10% forsterite. Dust opacity functions for these 3 cases are shown in Fig. A1.

In the case of C-rich stars, Suh (2000) prescribes mixtures of amorphous carbon (AMC) and silicon carbide (SiC), again in ratios that depend on the optical depth of the dusty shell. (*a*) For C-rich stars with optically thin shells ($\tau_{10} \leqslant 0.15$), 20% of SiC grains are needed to fit the strong 11 μm feature in observed spectra; (*b*) 10% of SiC grains are required for shells with intermediate optical depths ($0.15 < \tau_{10} \leqslant 0.8$), and (*c*) no SiC grains are necessitated at larger optical depths, for which the 11 μm feature is either weak or absent. Dust opacity functions for the 3 cases encountered for C-rich stars are displayed in Fig. A2.

Optical constants for the different grains are taken from Suh (1999, amorphous silicates), Suh (2000, amorphous carbon), Jaeger et al. (1998, enstatite), and Fabian et al. (2001, forsterite –actually, olivine: $Mg_{1.9}Fe_{0.1}SiO_4$). The data for α-SiC come from Pégourié (1988), and are included in DUSTY's built-in library of optical constants.

We take a uniform dust grain size of 0.1 μm, following Piovan et al. (2003). In general, for stars with $\dot{M} \neq 0$, we use DUSTY's numerical solution for radiatively driven winds, extending to a distance 10^4 times the inner radius. For $\tau \geqslant 80$, however, and due to numerical difficulties of the program, we assume a shell density distribution that falls off as r^{-2}. As for the incident radiation (that DUSTY surmises comes from a point source at the centre of the density distribution), we use the same stellar SEDs as the BC03 and CB09 standard models (adapted according to stellar parameters for modified mass-loss-rates), and for the dust temperature on the envelope inner boundary we input 1000 K for O-rich stars, and 1500 K for carbon stars (Marigo et al. 2008).[23] For consistency with Suh (1999, 2000, 2002) and Piovan et al. (2003), we evaluate κ_λ and τ_λ at 10μm, and naturally all our calculations with DUSTY take the same λ as their reference wavelength.

REFERENCES

Ajhar, E. A. & Tonry, J. L. 1994, ApJ, 429, 557

Ajhar, E. A., Lauer, T. R., Tonry, J. L., Blakeslee, J. P., Dressler, A., Holtzman, J. A., & Postman, M. 1997, AJ, 114, 626

Alongi, M., Bertelli, G., Bressan, A., Chiosi, C., Fagotto, F., Greggio, L., & Nasi, E. 1993, A& AS., 97, 851

Asplund, M., Grevesse, N., & Sauval, A. J. 2005, Cosmic Abundances as Records of Stellar Evolution and Nucleosynthesis, 336, 25

Baud, B., & Habing, H. J. 1983, A& A, 127, 73

Bertelli, G., Girardi, L., Marigo, P., & Nasi, E. 2008, A& A, 484, 815

Blakeslee, J. P., et al. 2009, ApJ, 694, 556

Blanco, A., Falcicchia, G., & Merico, F. 1983, Ap&SS, 89, 163

Bloecker, T. 1995, A& A, 297, 727

Bowen, G. H., & Willson, L. A. 1991, ApJL, 375, L53

Bressan, A., Fagotto, F., Bertelli, G., & Chiosi, C. 1993, A& AS., 100, 647

Bressan, A., Granato, G. L., & Silva, L. 1998, A& A, 332, 135

Bruzual A., G. 2002, in Extragalactic Star Clusters, IAU Symposium Ser., Vol. 207, eds. D. Geisler, E. K. Grebel, & D. Minniti (Provo:ASP), 616

Bruzual, G., 2007, in Proceedings of the IAU Symposium No. 241 "Stellar populations as building blocks of galaxies", eds. A. Vazdekis and R. Peletier, Cambridge: Cambridge University Press, 125 (arXiv:astro-ph 0703052)

Bruzual, G., & Charlot, S. 2003, MNRAS, 344, 1000

Charlot, S., & Bruzual, G. 2009, in preparation

Cantiello, M., Blakeslee, J. P., Raimondo, G., Mei, S., Brocato, E., & Capaccioli, M. 2005, ApJ, 634, 239

Cantiello, M., Raimondo, G., Brocato, E., & Capaccioli, M. 2003, AJ, 125, 2783

Cantiello, M., Blakeslee, J., Raimondo, G., Brocato, E., & Capaccioli, M. 2007, ApJ, 668, 130

---

[23] For the most massive stars ($M \gtrsim 4M_\odot$), both C-rich and O-rich, occasionally there are extremely short ($10 - 100$ yr long) phases with no mass-loss that follow mass-losing stages with a duration of $\sim 10^5$ yr. We worried that standard (i.e., Schultheis et al. or Westera et al., as appropriate) spectra would not provide a realistic modelling of such phases, and performed the experiment of assigning to them, instead, the spectra of the immediately preceding stage. The results of both procedures (standard spectra and preceding stage spectra) were indistinguishable for all practical purposes.

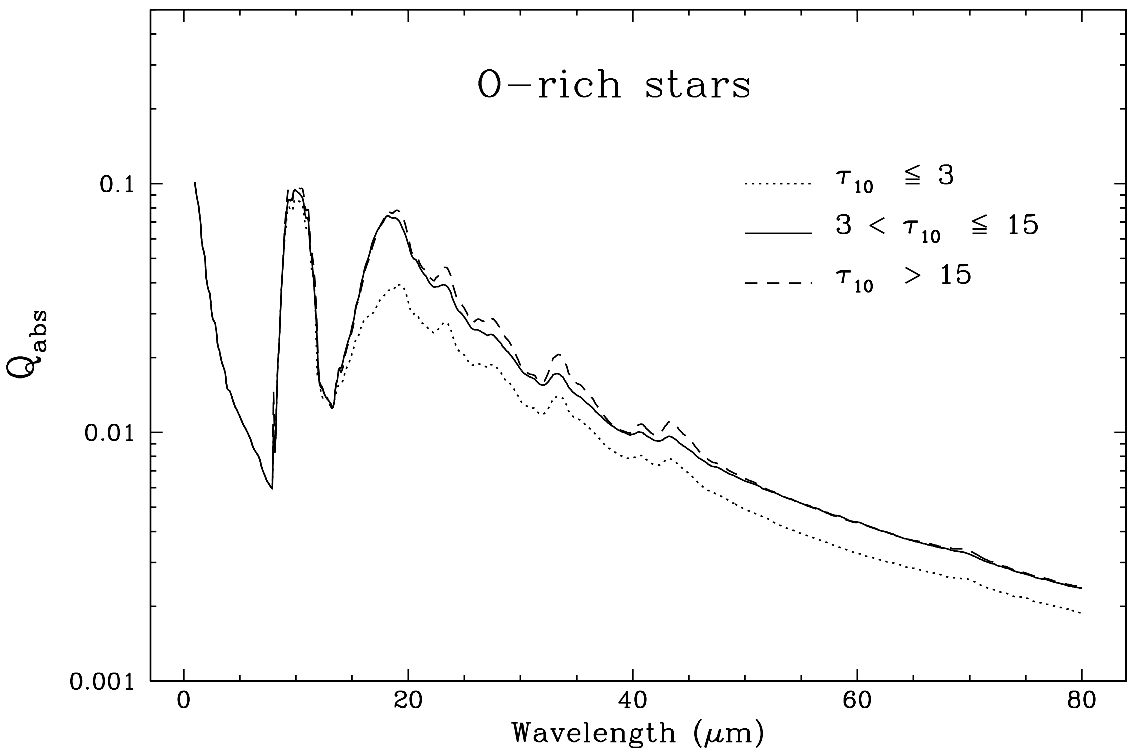

Figure A1. Absorption efficiency functions of different mixtures of siliceous dust grains, for envelopes of O-rich stars with various optical depths. *Dotted-line:* $\tau_{10} \leqslant 3$; *solid-line:* $3 < \tau_{10} \leqslant 15$; *dashed-line:* $\tau_{10} > 15$ (see text).

Cantiello, M., Raimondo, G., Blakeslee, J. P., Brocato, E., & Capaccioli, M. 2007, ApJ, 662, 940

Cerviño, Valls–Gabaud, Luridiana, & Mas–Hesse, J. M. 2002, A&A, 381, 51

Cerviño, M., & Luridiana, V. 2006, A& A, 451, 475

Chabrier, G. 2003, PASP, 115, 763

Cioni, M.-R., et al. 2000, VizieR Online Data Catalog, 2228, 0

Cohen, J. G. 1982, ApJ, 258, 143

de Jager, C., Nieuwenhuijzen, H., & van der Hucht, K. A. 1988, A& AS., 72, 259

Demleitner, M., Accomazzi, A., Eichhorn, G., Grant, C. S., Kurtz, M. J., & Murray, S. S. 2001, ASP Conf. Ser. 238: Astronomical Data Analysis Software and Systems X, 238, 32

Dorschner, J., Begemann, B., Henning, T., Jaeger, C., & Mutschke, H. 1995, A& A, 300, 503

Elitzur, M., & Ivezić, Ž. 2001, MNRAS, 327, 403

Elson, R. A. W. & Fall, S. M. 1985, ApJ, 299, 211

————————.1988, AJ, 96, 1383

Epchtein, N., et al. 1997, The Messenger, 87, 27

Fabian, D., Henning, T., Jäger, C., Mutschke, H., Dorschner, J., & Wehrhan, O. 2001, A& A, 378, 228

Fagotto, F., Bressan, A., Bertelli, G., & Chiosi, C. 1994, A& AS., 104, 365

————————.1994, A& AS., 105, 29

Ferrarese, L. et al. 2000, ApJS, 128, 431

Ferraro, F. R., Fusi Pecci, F., Testa, V., Greggio, L., Corsi, C. E., Buonanno, R., Terndrup, D. M., & Zinnecker, H. 1995, MNRAS, 272, 391

Ferrarotti, A. S., & Gail, H.-P. 2001, A& A, 371, 133

Ferrarotti, A. S. 2003, Ph.D. Thesis

Ferrarotti, A. S., & Gail, H.-P. 2006, A& A, 447, 553

Frogel, J.A., Mould, J., & Blanco, V.M., 1990, ApJ, 352, 96

Gail, H.-P., & Sedlmayr, E. 1986, A& A, 161, 201

Gallart, C., et al. 2003, AJ, 125, 742

Girardi, L., Chiosi, C., Bertelli, G., & Bressan, A. 1995, A& A, 298, 87

Girardi, L., Bressan, A., Chiosi, C., Bertelli, G., & Nasi, E. 1996, A& AS., 117, 113

Girardi, L., & Marigo, P. 2007, A& A, 462, 237

González, R. A., Liu, M. C., & Bruzual A., G. 2004, ApJ, 611, 270

————————.2005, ApJ, 621, 557

González-Lópezlira, R. A., Albarrán, M. Y., Mouhcine, M., Liu, M. C., Bruzual-A., G., & de Batz, B. 2005, MNRAS, 363, 1279

González-Lópezlira, R. A., & Buzzoni, A. 2007, in Ultraviolet properties of evolved stellar populations, eds.

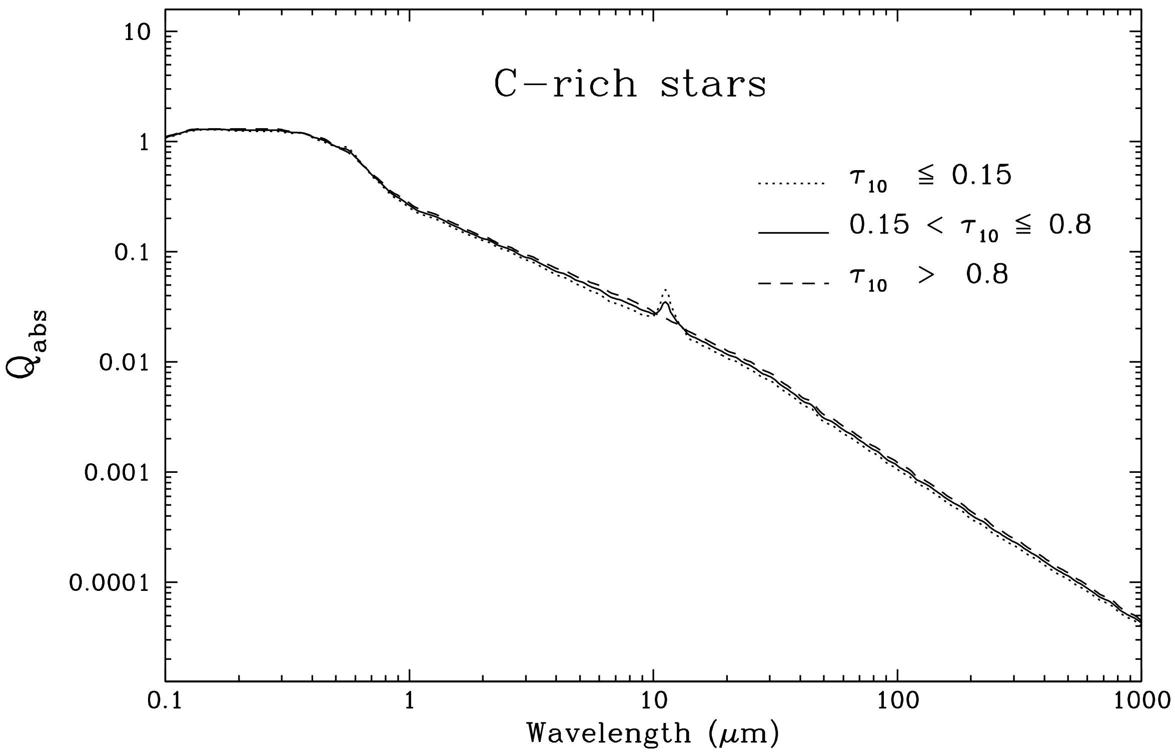

Figure A2. Absorption efficiency functions of different mixtures of carbonaceous dust grains, for envelopes of C-rich stars with various optical depths. *Dotted-line:* $\tau_{10} \leqslant 0.15$; *solid-line:* $0.15 < \tau_{10} \leqslant 0.8$; *dashed-line:* $\tau_{10} > 0.8$ (see text).

M. Chávez, E. Bertone, D. Rosa-González, & L. H. Rodríguez-Merino, Astrophysics and Space Science Proceedings (Dordrecht:Springer), in press (arXiv:astro-ph 0708.0193)

Grevesse, N., & Sauval, A. J. 1998, Space Science Reviews, 85, 161

Groenewegen, M. A. T., & de Jong, T. 1994, A& A, 288, 782

Groenewegen, M. A. T., Smith, C. H., Wood, P. R., Omont, A., & Fujiyoshi, T. 1995, ApJL, 449, L119

Iben, I., Jr. 1984, ApJ, 277, 333

Iben, I., Jr., & Renzini, A. 1983, ARA&A, 21, 271

Ivezić, Z., & Elitzur, M. 1997, MNRAS, 287, 799

Ivezić, Z., Nenkova, M., & Elitzur, M. 1999, User Manual for DUSTY, University of Kentucky Internal Report (`http://www.pa.uky.edu/~moshe/dusty`)

Jaeger, C., Molster, F. J., Dorschner, J., Henning, T., Mutschke, H., & Waters, L. B. F. M. 1998, A& A, 339, 904

Jensen, J. B., Tonry, J. L., Barris, B. J., Thompson, R. I., Liu, M. C., Rieke, M. J., Ajhar, E. A., & Blakeslee, J. P. 2003, ApJ, 583, 712

Kalirai, J. S., Hansen, B. M. S., Kelson, D. D., Reitzel, D. B., Rich, R. M., & Richer, H. B. 2008, ApJ, 676, 594

Kalirai, J. S., Richer, H. B., Reitzel, D., Hansen, B. M. S., Rich, R. M., Fahlman, G. G., Gibson, B. K., & von Hippel, T. 2005, ApJL, 618, L123

Knapp, G. R. 1985, ApJ, 293, 273

Kuntschner, H. 1998, Ph.D. thesis, University of Durham, UK.

Lançon, A., & Mouhcine, M. 2002, A& A, 393, 167

Lebzelter, T., Posch, T., Hinkle, K., Wood, P. R., & Bouwman, J. 2006, ApJL, 653, L145

Lepine, J. R. D., Ortiz, R., & Epchtein, N. 1995, A& A, 299, 453

Liu, M. C., Charlot, S., & Graham, J. R. 2000, ApJ, 543, 644

Liu, M. C., Graham, J. R., & Charlot, S. 2002, ApJ, 564, 216

Lyubimkov, L. S., Rostopchin, S. I., Rachkovskaya, T. M., Poklad, D. B., & Lambert, D. L. 2005, MNRAS, 358, 193

Maraston, C. 1998, MNRAS, 300, 872

________________.2005, MNRAS, 362, 799

Maraston C., Daddi E., Renzini A., Cimatti A., Dickinson M., Papovich C., Pasquali A., & Pirzkal, N. 2006, ApJ, 652, 85; (Erratum: 2007, ApJ, 656, 1241)

Marigo, P., Bressan, A., & Chiosi, C. 1996, A& A, 313, 545

Marigo, P., & Girardi, L. 2007, A& A, 469, 239

Marigo, P., Girardi, L., Bressan, A., Groenewegen, M. A. T., Silva, L., & Granato, G. L. 2008, A& A, 482,

883
Marín-Franch, A., & Aparicio, A. 2006, A& A, 450, 979
Mei, S., Quinn, P. J., & Silva, D. R. 2001, A& A, 371, 779
Mei, S., et al. 2005, ApJS, 156, 113
————————.2005, ApJ, 625, 121
————————.2007, ApJ, 655, 144
Mighell, K. J., Rich, R. M., Shara, M., & Fall, S. M. 1996, AJ, 111, 2314
Mokiem, M. R., et al. 2007, A& A, 473, 603
Mouhcine, M., González, R. A., & Liu, M. C. 2005, MNRAS, 362, 1208
Mouhcine, M., & Lançon, A. 2003, A& A, 402, 425
Pahre, M. A., & Mould, J. R. 1994, ApJ, 433, 567
Pégourié, B. 1988, A& A, 194, 335
Piovan, L., Tantalo, R., & Chiosi, C. 2003, A& A, 408, 559
Raimondo, G. 2009, ApJ, 700, 1247
Raimondo, G., Brocato, E., Cantiello, M., & Capaccioli, M. 2005, AJ, 130, 2625
Reimers, D. 1975, Memoires of the Societe Royale des Sciences de Liege, 8, 369
————————.1977, A& A, 61, 217
Renzini, A., & Buzzoni, A. 1986, Spectral Evolution of Galaxies, 122, 195
Renzini, A., & Voli, M. 1981, A& A, 94, 175
Russell, S. C., & Bessell, M. S. 1989, ApJS, 70, 865
Santos, J. F. C., & Frogel, J. A. 1997, ApJ, 479, 764
Schultheis, M., Aringer, B., Jorgensen, U. G. Lebzelter, T., & Plez, B. 1999, Abstract of the 2nd Austrian ISO workshop: Atmospheres of M, S, and C Giants, eds. J. Hron & S. Höfner, 93
Searle, L., Wilkinson, A., & Bagnuolo, W. G. 1980, ApJ, 239, 803
Skrutskie, M. F. et al. 1997, ASSL Vol. 210: The Impact of Large Scale Near–IR Sky Surveys, 25
Steffen, M., Szczerba, R., Men'shchikov, A., & Schoenberner, D. 1997, A& AS., 126, 39
Suh, K.-W. 2002, MNRAS, 332, 513
————————.2000, MNRAS, 315, 740
————————.1999, MNRAS, 304, 389
Srinivasan, S., et al. 2009, AJ, 137, 4810
Tonry, J. L., Ajhar, E. A., & Luppino, G. A. 1990, AJ, 100, 1416
Tonry, J. L., Blakeslee, J. P., Ajhar, E. A., & Dressler, A. 1997, ApJ, 475, 399
Tonry, J. L., Dressler, A., Blakeslee, J. P., Ajhar, E. A., Fletcher, A. B., Luppino, G. A., Metzger, M. R., & Moore, C. B. 2001, ApJ, 546, 681
Tonry, J. & Schneider, D. P. 1988, AJ, 96, 807
van den Bergh, S. 1981, A&AS, 46, 79
van Loon, J. T. 2000, A& A, 354, 125
————————.2006, Stellar Evolution at Low Metallicity: Mass Loss, Explosions, Cosmology, 353, 211
van Loon, J. T., Cioni, M.-R. L., Zijlstra, A. A., & Loup, C. 2005, A& A, 438, 273
Vassiliadis, E. & Wood, P. R. 1993, ApJ, 413, 641
Wachter, A., Schröder, K.-P., Winters, J. M., Arndt, T. U., & Sedlmayr, E. 2002, A& A, 384, 452
Westera, P., Lejeune, T., Buser, R., Cuisinier, F., & Bruzual A., G. 2002, A& A, 381, 524
Willson, L. A. 2000, ARA&A, 38, 573
Worthey, G. 1993a, ApJ, 415, 91
————————.1993b, ApJ, 418, 947